Instituto Tecnológico de Costa Rica

Escuela de Ingeniería Electrónica

Programa de Maestría en Ingeniería Electrónica con Énfasis en Sistemas Microelectromecánicos

"Equivalent circuit modeling for electrochemical impedance spectroscopy"

Tesis de graduación para optar por el título de

Magister Scientiae en Ingeniería Electrónica
Énfasis en Sistemas Microelectromecánicos

con el grado académico de

Maestría

Juan José Montero-Rodríguez

Hamburgo, Diciembre 2013

Instituto Tecnológico de Costa Rica

Electronics Engineering Department

Master's Thesis

Examination Commitee

Master's degree thesis reviewed by the present Examination Commitee as a requirement to qualify for the Master's Degree in Electronics Engineering with emphasis on Microelectromechanical Systems at the Instituto Tecnológico de Costa Rica.

Commitee Members

Prof. Dr.-Ing. Wolfgang Krautschneider

Director, Institute of Nanoelectronics,

Technische Universität Hamburg-Harburg

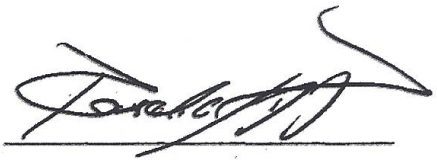

M.Sc. Ricardo Starbird-Pérez

Advisor

M.Sc. Gabriela Ortiz-León

Reviewer

M.Sc. Mario Meza-Cuevas

Reviewer

The members of this Commitee attest that this graduate work has been approved and meets the standards set by the Electronics Engineering Department.

Hamburg, Germany

December 05, 2013

INSTITUTO TECNOLOGICO DE COSTA RICA
ESCUELA DE INGENIERIA ELECTRONICA
PROYECTO DE GRADUACIÓN
TRIBUNAL EVALUADOR
ACTA DE EVALUACIÓN

Proyecto de Graduación defendido ante el presente Tribunal Evaluador como requisito para optar por el grado académico de Maestría en Electrónica con énfasis en Sistemas Microelectromecánicos, del Instituto Tecnológico de Costa Rica.

Estudiante: Juan José Montero Rodríguez

Carné: 200746910

Nombre del Proyecto: Equivalent Circuit Modeling for Electrochemical Impedance Spectroscopy

Miembros del Tribunal

Prof. Dr-Ing. Wolfgang Krautschneider

Director, Instituto de Nanoelectrónica, Technische Universität Hamburg-Harburg

M.Sc. Ricardo Starbird-Pérez

Profesor asesor

M.Sc. Gabriela Ortiz-León

Profesor lector

M.Sc. Mario Meza-Cuevas

Profesor lector

Los miembros de este Tribunal dan fe de que el presente trabajo de graduación ha sido aprobado y cumple con las normas establecidas por la Escuela de Ingeniería Electrónica

Nota Final del Proyecto de Graduación : 95

05 de diciembre de 2013

Resumen

El diseño y fabricación de electrodos neurales implantables es un reto, debido a que los materiales y las interfaces deben proveer una baja resistencia a los tejidos, con una alta capacidad de inyección de corriente. En el Instituto de Materiales Ópticos y Electrónicos de la Universidad Técnica de Hamburgo, los investigadores han encontrado una forma de estructurar capas delgadas de polímeros conductores sobre electrodos de oro, mejorando la interfaz entre el metal y los tejidos. La presente tesis trata sobre la caracterización eléctrica de electrodos metálicos cubiertos con capas delgadas de PEDOT:PSS. Un conjunto de 96 electrodos individuales con distinta área superficial y espesor de polímero ha sido medido mediante espectroscopía de impedancia electroquímica. El objetivo de la presente tesis es desarrollar un modelo equivalente para la interfaz metal/polímero/tejido, y ajustar los datos experimentales a este modelo para explorar las distintas capacitancias y resistencias de la interfaz. Un total de seis modelos fueron obtenidos de la literatura, y se implementaron para ajustar los datos usando herramientas comerciales estándar, como MEISP de Kuhmo Petrochemical, o LEVMW de J.R. Macdonald. La conclusión de este trabajo es que la capacitancia entre el polímero y la solución, también llamada capacitancia de doble capa, aumenta linealmente con el espesor del polímero, y es más alta que la capacitancia en la interfaz metal/polímero.

Palabras clave: electrodos, espectroscopía de impedancia, modelo matemático, polímeros conductores

Abstract

The design and fabrication of implantable neural electrodes is a challenge, because the materials and interfaces must provide low impedance to the tissues, with high current injection capabilities. In the Institute of Optical and Electronic Materials, researchers have found a way to structure thin layers of conductive polymers on top of gold electrodes, improving the interface between metal and tissues. This thesis deals with the electrical characterization of metallic electrodes coated with thin layers of PEDOT:PSS. A set of 96 individual electrodes with different surface area and polymer thickness was measured by electrochemical impedance spectroscopy. The goal of the present thesis is to develop an equivalent model for the metal/polymer/tissue interface, and fit the experimental data to this model to explore the different capacitances and resistances of the interface. A total of six models were obtained from literature, and they were implemented to fit the data using standard commercial tools such as MEISP from Kuhmo Petrochemical, or LEVMW from J.R. Macdonald. The main conclusion is that the polymer/solution capacitance, also called the double-layer capacitance, increases linearly with the thickness of the polymeric layer, and it is higher than the metal/polymer capacitance.

Key words: conductive polymers, electrodes, impedance spectroscopy, mathematical modeling

Declaration of authenticity

I declare that the present dissertation is my original work, and has been developed with available references using my own knowledge. It has not been previously submitted to any other university for a higher degree.

I also declare that the publications cited in this work have been personally consulted. Then I assume complete responsibility for the present thesis and for the contents of the final report.

Juan José Montero-Rodríguez
Passport: 1-1348-0574
Hamburg, Germany
December 5th, 2013

Contents

List of Figures

Chapter 1

Introduction

Conductive polymers (CP) are a special class of polymeric materials with particular electrical, mechanical, optical and thermal properties. They can be doped to control their conductivity [1], they are not toxic [2] and the fabrication method has been studied since 1976 [3], which makes them suitable for biomedical applications such as neural recording and stimulation, controlled drug release, improvement of implantable electrodes and devices, and development of artificial muscles and prosthesis [4].

A collaborative research group is working on this subject at the Technische Universität Hamburg-Harburg (TUHH), involving researchers from the Institut für Nanoelektronik and the Institüt fur Optische und Elektronische Materialen. The project is conducted by Prof. Dr.-Ing. Wolfgang Krautschneider and Prof. Dr.-Ing. Wolfgang Bauhofer. They are working on polymeric coatings for implantable neural electrodes, in order to achieve better electrical behavior and mechanical performance [5].

Researchers at the TUHH have fabricated gold electrodes on a polyimide substrate, and coated them with uniform layers of poly(3,4-ethylenedioxythiophene) (PEDOT). Electrodes have different sizes (0,5; 1,0 and 2,0 mm^2) and different polymer thicknesses. The thickness of the polymer can be controlled by adjusting the charge density (CD) at polymerization time. We have experimental data for four different charge densities (0; 40; 80 and 120 mC/cm^2).

To measure the electrical performance of the polymer-coated electrodes, researchers have used Electrochemical Impedance Spectroscopy (EIS). In these in-vitro experiments, the electrode is immersed in an aqueous solution representing the tissues. An AC signal is applied to the electrode, and the impedance is measured at different frequencies, obtaining a Bode plot. This technique enables the study of the metal/polymer/solution interfaces present in the experiment.

Results from EIS measurements can be used to obtain information about the physical system and the interfaces. One method commonly used in the literature is to fit the experimental data to a mathematical model. These models are built with equivalent circuit elements (for example: resistances, capacitances, inductances) and each component has a physical meaning. The elements can be extracted from the experimental frequency responses, using numerical methods and algorithms.

In this master's thesis we need to fit the experimental EIS data to a mathematical model with physical significance. The model should describe the metal/polymer and the polymer/solution interfaces and explain the differences between electrodes fabricated with different sizes and charge densities.

For example, experimental data for eight electrodes is plotted in Figure 1. In this experiment the electrodes have a surface area of 2,0 mm^2, and the charge density is fixed to 120 mC/cm^2 for electrodes 1, 2, 3, 6, 7 and 8. In the same plots, electrodes 4 and 5 are reference electrodes and do not have any coating. This is referenced as a charge density of 0 mC/cm^2.

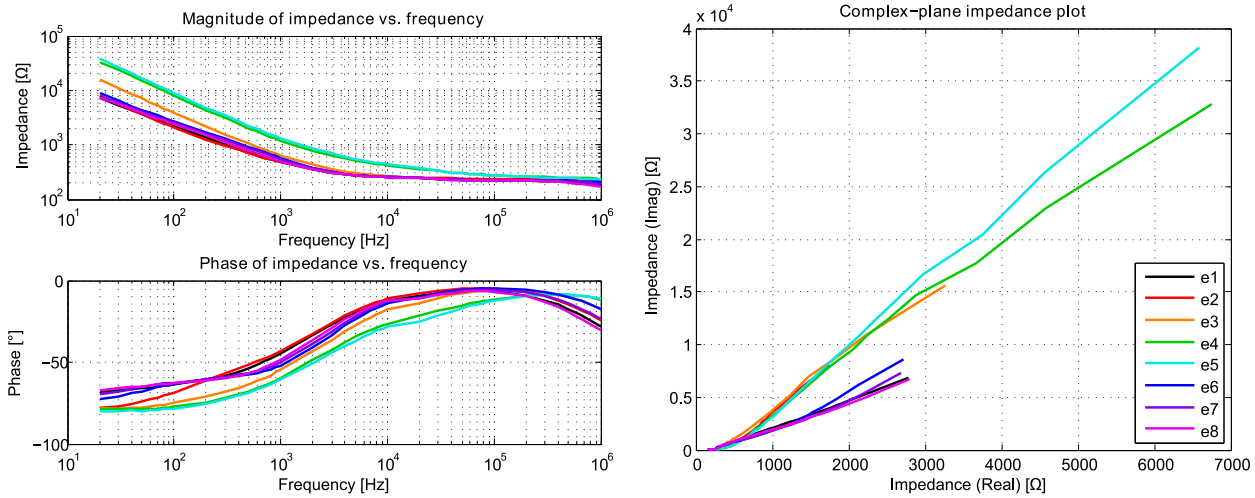

(a) Bode plots of sample “Au20T01”.

(b) Nyquist plots of sample “Au20T01”.

Figure 1: Bode and Nyquist plots of experimental data for test sample “Au20T01”.

As can be seen from these graphics, the reference electrodes 4 and 5 have higher impedance when compared to the polymer-coated electrodes. With an equivalent circuit model we can explain the physical phenomena at the interfaces of the metal/polymer/solution system, and justify the differences in these impedance plots.

1.1 Thesis structure

This thesis is divided in three sections. The first section is a literature review of mathematical models used to describe the metal/polymer/aqueous interfaces. This includes the description of six equivalent circuit models, which are physically significant because they are built using circuit elements. For example, resistances in these models describe conduction processes, and capacitances represent charge accumulation at the interfaces.

The second part of the thesis is the model fitting and the extraction of circuit elements, starting from EIS experimental data. The fitting process is performed using two different tools: Macdonald’s LEVMW 8.12 and Kuhmo Petrochemical ltd. MEISP 3.0. Both programs apply nuerical methods to extract the circuit parameters from the frequency response of the electrodes.

The third part of this document is the model validation and statistical analysis of the achieved fitting results. We fabricated a new set of electrodes with different deposition conditions, and then compared the fitting results with the extrapolated data using linear regression. Some statistical tools used were the Dixon’s Q-test for outlier detection, and the one-way ANOVA for selecting the model with the best trend for the physical parameters.

Chapter 2

Objectives

2.1 General objective

Improvement of the electrical performance of conductive-polymer coated gold electrodes.

2.2 Specific objectives

1. Model the system metal/polymer/tissue.
   (a) Study equivalent circuits often used for polymer/tissue simulations.
   (b) Model the system polymer/tissue using MATLAB®.
2. Fit the experimental data of impedance spectroscopy to selected mathematical models.
   (a) Apply statistical methods to validate the parameters from the model.
   (b) Correlate the value of the obtained parameters with real values.
3. Validate the model using different deposition conditions.
   (a) Calculate the expected parameters for the model using different charge densities.
   (b) Fabricate an electrode with the selected deposition charge densities.
   (c) Compare calculated data with experimental data.

Chapter 3

Theoretical background

This chapter describes the theory of Electrochemical Impedance Spectroscopy (EIS) and how this technique is used to characterize the neural electrodes in an *in vitro* study.

The first part of this chapter is the description of the physical system used to reproduce the conditions of an implanted electrode, surrounded by tissues. Here we describe the details of the gold/polymer/solution interfaces and the experimental procedure required to perform an EIS experiment and obtain impedance curves.

The second part of this chapter includes the possible formats that can be used for presenting and visualizing the results of an EIS measurement.

The third section of this chapter explains the importance of mathematical modeling for Electrochemical Impedance Spectroscopy, and one of the limitations of equivalent circuit models. Here we explain five circuit elements used to model electrochemical systems: resistance, capacitance, inductance, the Warburg element and the Constant phase element.

The fourth part of this chapter is a review of mathematical software used to fit the data, starting from the Bode and Nyquist plots. Here we describe J.R. Macdonald's LEVMW software, MEISP 3.0 and some other free and commercial software tools that can be used to fit the data.

3.1 Description of the physical system

This thesis is focused on the characterization of implantable electrodes for nerve stimulation and signal recording. These electrodes are usually fabricated in the form of small needles, allowing direct implantation by injecting the active part in the tissue. One example of an implantable electrode was achieved by K. Cheung [6][7] and can be appreciated in Figure 2a. The electrodes are usually coated with conductive polymers to improve their electrical performance.

To study the impact of different fabrication parameters on the impedance of the electrodes, the research group at the TUHH produced larger versions of electrodes in a polyimide substrate. Larger electrodes are easier to fabricate, can be produced in less time, and they are less expensive. The electrodes used for this master's thesis are shown in Figure 2b.

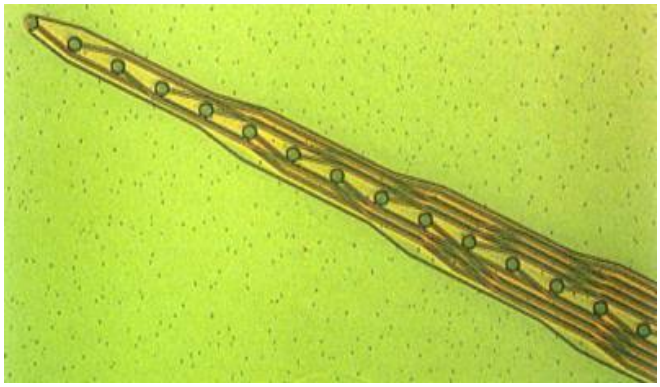

(a) Brain electrode by K. Cheung [6][7].

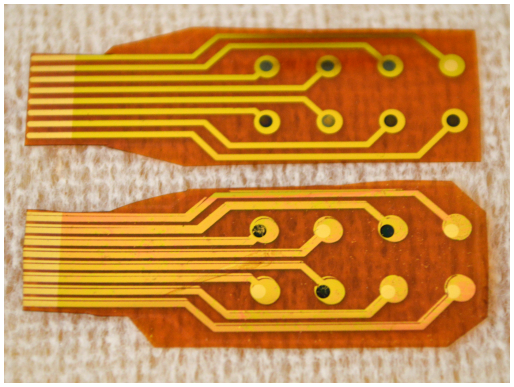

(b) Sample electrodes for this thesis.

Figure 2: Implantable electrodes for neural recording/stimulation.

The main function of these electrodes is to provide a low-resistance path to contact tissues or nerves in the brain, enabling neurologists to record signals with better quality. At the TUHH we required to measure the electrical performance of these electrodes, by reproducing the experimental conditions of the implanted electrode in an *in vitro* study. When implanted in the brain, the electrodes will be surrounded by tissues and nerves, which can be replaced with a saline aqueous solution for experimental purposes.

With an artificial representation of the implanted electrode, we can manually adjust the fabrication parameters and observe the changes in electrode performance. There are two important parameters studied in this thesis: the effective **surface area** (A) of the electrode, and the conductive polymer coating thickness, which is proportional to the **charge density** (CD) used at polymerization time.

In order measure the electrode performance, researchers at the TUHH have used Electrochemical Impedance Spectroscopy (EIS). This technique studies the impedance of an electrochemical system, by sweeping the frequency of an input voltage and measuring the current through the electrode [8][9]. Impedance spectroscopy is of interest because it can describe the effect of each individual interface.

The experimental setup comprises a metallic test chamber connected to ground (reference), an aqueous solution representing the tissues, the sample electrode under test (work electrode), and a conductive polymer coating on the surface of this working electrode. The experimental chamber currently used in the laboratory is shown in Figure 3a, and an example of a commercial test chamber from Metrohm Autolab is shown in Figure 3b.

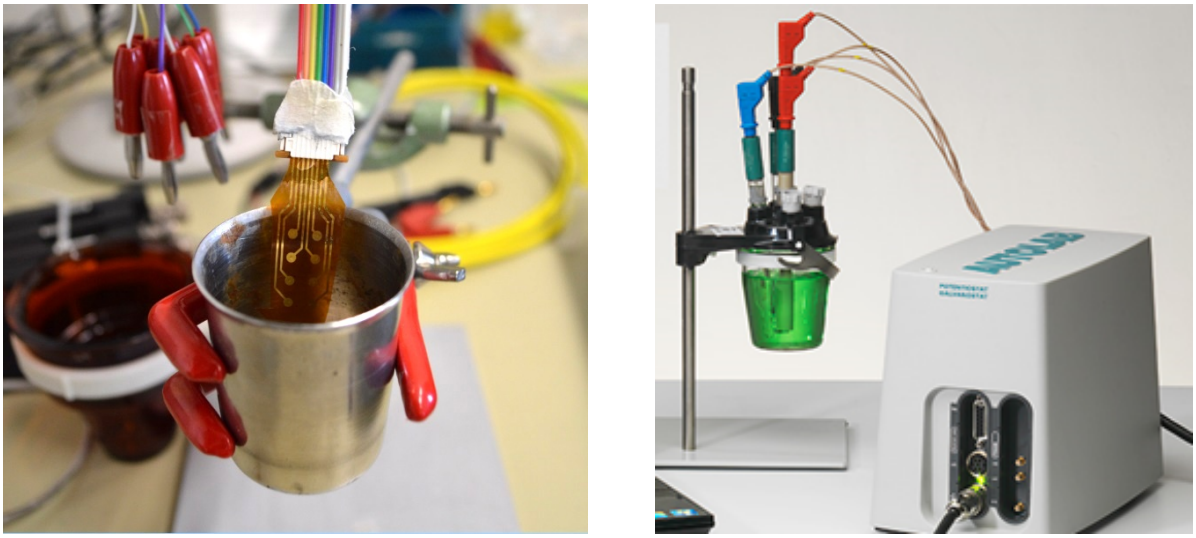

(a) Measurement chamber used in this thesis. (b) Commercial tool from Metrohm Autolab.

Figure 3: Examples of a test cell.

The experimental procedure is as follows: the reference electrode is connected to a ground potential, and then a square input voltage of 50 mV is applied selectively to one of the eight working electrodes. The remaining seven electrodes are left floating, to remove them from the system completely. The frequency of the input signal is sweeped from 20 Hz up to 1 MHz, and the electrical current through the electrode is measured, to calculate the impedance of the electrode.

The schematic representation of the experimental setup can be observed in Figure 4a. Gold electrodes are covered with conductive polymer coatings of different thicknesses, and are immersed in a commercial irrigation solution representing the tissues. The thickness of the polymeric coatings is controlled by the charge density (CD) during the time of polymer deposition. There are eight gold electrodes for each experiment, and the thickness can be adjusted independently when they are fabricated. For all the electrodes used in this study, the conductive polymer is poly(3,4-ethylenedioxythiophene) doped with poly(styrenesulfonate), abbreviated as PEDOT-PSS.

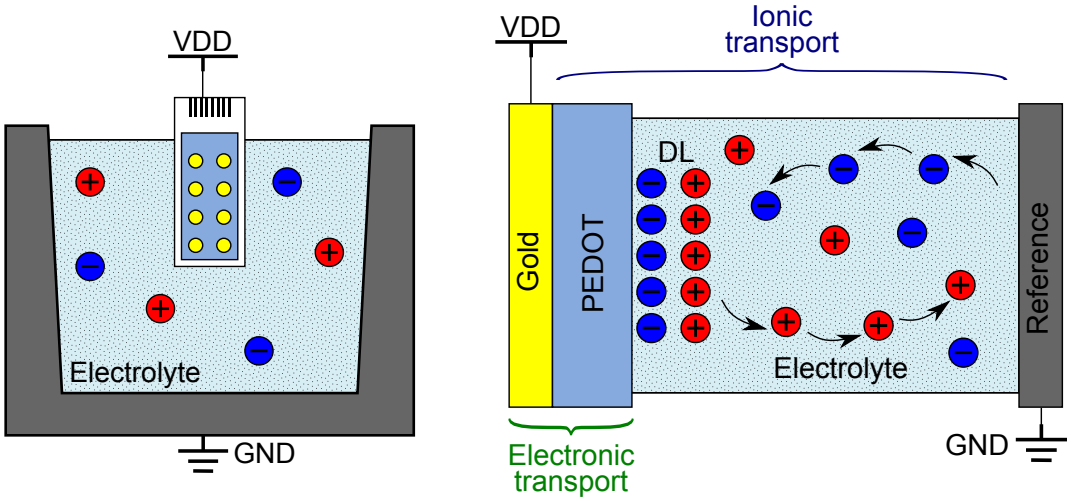

(a) Experimental setup. (b) Charge transfer mechanism.

Figure 4: Experimental configuration for EIS.

Figure 4b is a magnification of a single gold electrode from Figure 4a. The electrode is coated with a polymeric layer, as can be seen in this horizontal representation, and the polymer is in direct contact with the solution. This representation is valid for one independent electrode, when all the remaining seven electrodes are ommited and disconnected from the system.

There are two interfaces present in this experimental setup. An interface is defined as the region of space between two different materials, and they are important in this electrochemical system because charge must be transferred from one material to the other, in order to reach the tissues. The first interface is the **metal/polymer** interface, where the predominant charge carriers are the electrons present in the gold electrode. The second is the **polymer/tissue** interface: an electrochemical reaction takes place in the polymer, where the electrons are attached to the polymeric structure, releasing ions into the aqueous solution [3]. This reaction is reversible, meaning that the electrode can be used for neural recording and neural stimulation, reversing the direction of the charge flow.

The reason why this metal/polymer/solution system exhibits lower impedance than a gold electrode directly in contact with the solution, is because the conductive polymer exhibits both electronic and ionic charge transfer mechanisms at the same time, and is actively transferring electrons from the gold electrode to ions in the electrolyte. The conversion between electrons and ions is based on a Reduction-Oxidation reaction (RedOx) which takes place at the electrode surface when the polymer is stimulated by electrons. The reaction mechanisms and a detailed explanation of the conduction process is found in A. Heeger [3].

3.2 Electrochemical Impedance Spectroscopy

Electrochemical Impedance Spectroscopy (EIS) studies the impedance of an electrochemical system as a function of the frequency of the applied signal.

There are different ways to report the impedance results of an EIS experiment. The most common output plot is the Bode plot, and can be represented in polar coordinates (magnitude and phase of the impedance) or in rectangular coordinates (real and complex part of the impedance). These representations are shown in Figure 5.

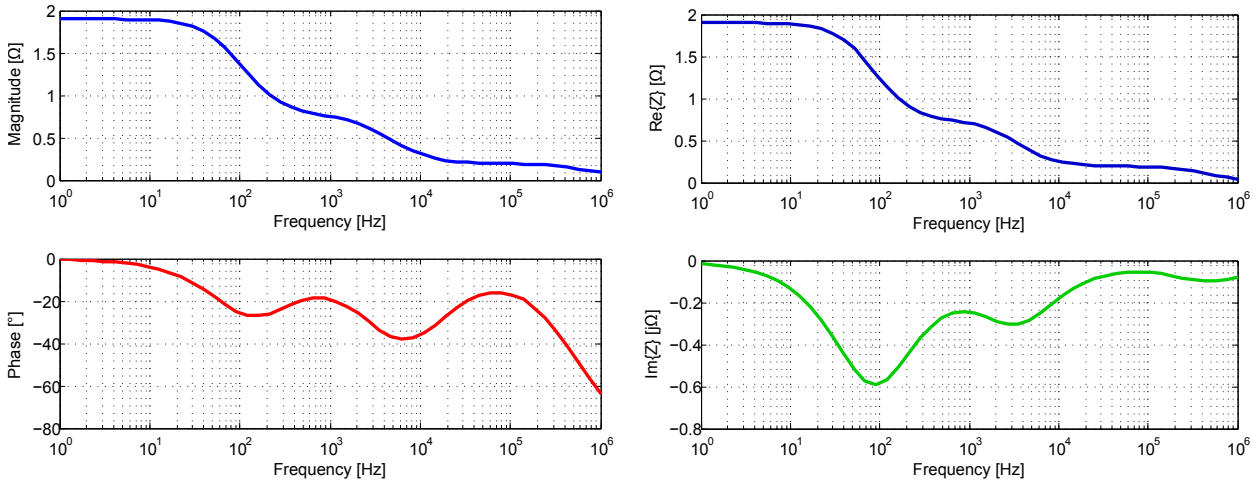

(a) Bode plot (polar).

(b) Bode plot (rectangular).

Figure 5: Representations of the impedance data as a function of the frequency.

Another way of representing the same data is by plotting the imaginary part of the impedance versus the real part of the impedance, placing one point for each frequency value. This plot is called the Nyquist plot, and an example is shown in Figure 6a. The Bode plot in rectangular coordinates, the Bode plot in polar coordinates, and the Nyquist plot are equivalent because they contain exactly the same amount of data. Results from an EIS experiment can be converted to any of these forms of visualization.

The impedance information can also be represented with a three-dimensional plot, where the x-axis is the frequency, the y-axis is the real part of the impedance, and the z-axis is the imaginary part, as can be seen in Figure 6b. Three-dimensional plots are useful because they contain the Bode and Nyquist diagrams in a single graphic. The xy-plane and the xz-plane are the Bode diagrams in rectangular coordinates (real part and complex part respectively), and the yz-plane is the Nyquist diagram.

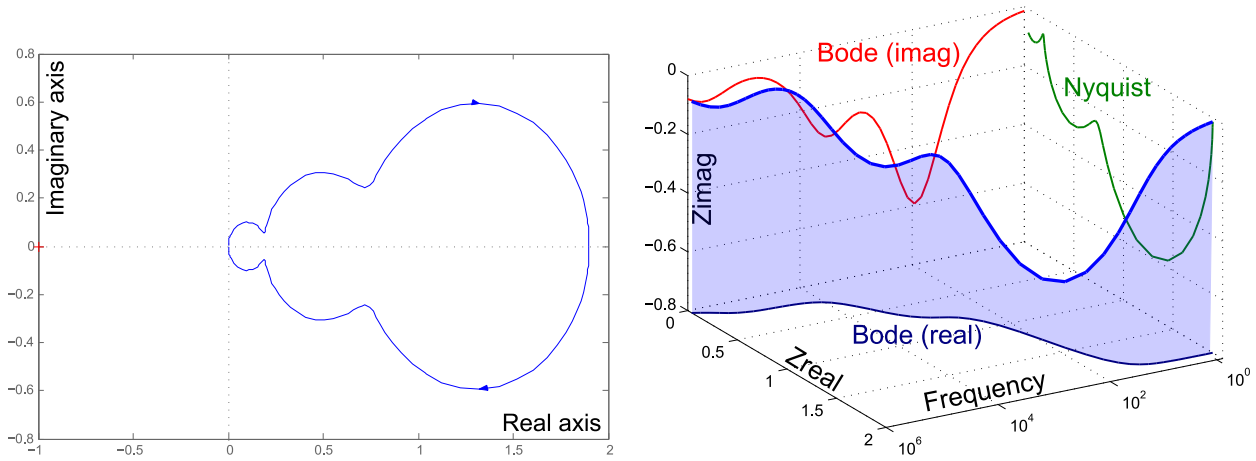

(a) Nyquist plot.

(b) Three-dimensional plot.

Figure 6: Alternate plots of the impedance data.

Further analysis of the EIS results is often required to obtain more information of the physical processes. This is achieved by fitting the experimental results to an equivalent circuit model, in which every element represents a conduction process or an interface. In the following section we explain five circuit elements that can be used to design the equivalent model, and discuss the main limitation of the method.

3.3 Mathematical models for EIS

Mathematical models and data fitting can be used to obtain several parameters related to the physical system. With a proper model, it is possible to calculate resistances, capacitances, describe the interfaces and explain electrochemical conditions present at the time of the fabrication, testing and normal operation of the electrodes.

The standard tools used to perform EIS measurements are potentiostats and galvanostats. Potentiostats apply a fixed AC voltage to the measured system, and galvanostats apply a fixed AC current, measuring the alternate variable while sweeping the frequency. We do not have access to a potentiostat or galvanostat at our institution, but we have measured the impedance of the electrodes as a function of the frequency with an Agilent 4284A LCR meter, and this data can be used to describe and obtain the equivalent parameters by fitting with numerical algorithms.

Mathematical modeling and fitting techniques are often available in the software of modern potentiostats and galvanostats, but the researcher should have knowledge of the physical system before starting the fitting process. his master's thesis includes the physical description of mathematical models, using equivalent circuit elements with physical significance.

There are five basic circuit elements that can be used in the experimental fitting process [10]. These circuit elements are the resistance, capacitance, inductance, the Warburg element and the constant phase element. A brief description of these elements is shown in Table 3.1, with the respective symbol and characteristic equation in the frequency domain.

Table 3.1: Basic circuit elements used in electrochemical impedance spectroscopy.

Parameter	Resistance (R)	Capacitance (C)	Inductance (L)	Warburg element (W)	Constant phase element (CPE)
Symbol					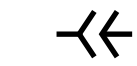
Equation	R	$\frac{1}{j\omega C}$	$j\omega L$	$\sigma\omega^{-1/2} - j(\sigma\omega^{-1/2})$	$q^{-1}(j\omega)^{-n}$

- **Resistance (R)** is present in aqueous solutions (ionic resistance), in electrodes and metallic parts (electronic resistance), and at the interfaces between electronic and ionic sections (charge transfer resistance).
- **Capacitance (C)** can be observed when there is charge accumulation in low-conductive media between two electrodes. There is usually one capacitor associated with each interface present in the system.
- **Inductance (L)** is the result of adsorption on the electrode surface, and it is not used as often as the rest of the elements.
- The **Warburg element (W)** is related to the diffusion of ions in the polymer/electrolyte interface, and it is the equivalent circuit of a transmission line with infinite RC elements. Ions move slower than electrons, and the solution affects the phase of the injected signals. There can be also reflections and propagations, described by the short-circuit Warburg (Ws) and the open-circuit Warburg (Wo) respectively.
- The **Constant phase element (CPE)** is used to describe a capacitive element that is distributed along a porous interface, such as a membrane or a porous material.

3.3.1 Critical issues related with EIS model fitting

One limitation of EIS model fitting is that many different equivalent circuits can be used to reproduce the same experimental data, and all of them are going to be mathematically correct [11]. An example was given by J.R. Macdonald [12], showing that the four circuits in Figure 7 exhibit the same frequency responses and are mathematically equivalent. This is because these circuits have exactly two capacitors and two resistances each, and the partial differential equations can be rewritten in the same canonical forms, selecting the appropriate constants. Here the author calculated the values for resistances and capacitances with numerical methods, starting with an arbitrary value assignment for circuit a).

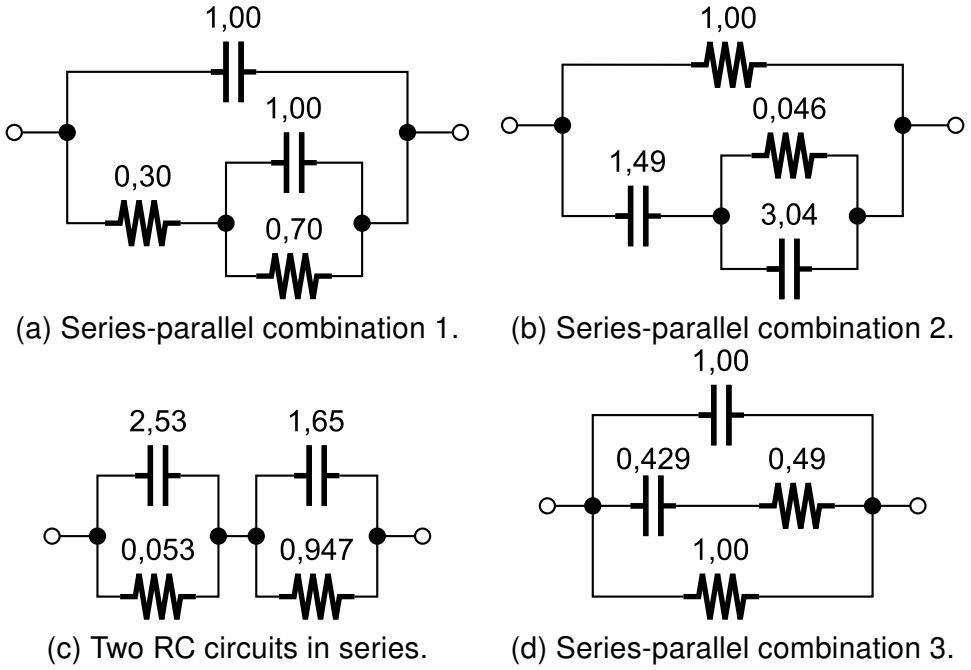

(a) Series-parallel combination 1. (b) Series-parallel combination 2.

(c) Two RC circuits in series. (d) Series-parallel combination 3.

Figure 7: Four equivalent circuits that exhibit the same impedance response.

The suggested approach to select the correct equivalent circuit according to the physical system can be summarized in the following steps:

1. Describe theoretically the physical system and the interfaces.
2. Check if charge is accumulated at the interfaces. Place a capacitor (in parallel with a resistance if the interface is conductive) to represent this behavior.
3. Assign simple circuit elements to each known charge transfer mechanism. For example, a resistance can be placed as the equivalent solution resistance of the aqueous part, because it should be constant at every frequency.
4. Identify other expected parameters that should be present in the circuit, by observing the shape of the Nyquist plots. More information about fitting Nyquist diagrams can be found at [13].
5. Fit the data to the selected model.

3.4 Fitting software and numerical methods

There are different fitting tools that allow the extraction of the passive elements from the Bode plots. Fitting software include numerical algorithms such as the Levenberg-Marquardt Algorithm (LMA), the Gauss-Newton Algorithm (GNA) and other Complex Nonlinear Least Squares (CNLS) methods.

Two non-commercial tools that were found in the literature were the James Ross Macdonald's LEVMW, and the Kuhmo Petrochemical ltd. MEISP 3.0, which was discontinued and can be used free of charge for non-commercial purposes. They are used to perform the fittings in this master's thesis. Another software used was the EIS Spectrum Analyzer, which includes a model library with a bibliographical database.

There are also many commercial tools that can be used to perform the fittings, for example: NOVA by Metrohm Autolab, PowerSINE from Princeton Applied Research, EIS300 from Gamry Instruments, and Zview from Scribner Associates, among many other licensed software. The algorithms used in these tools are similar to the ones included in the free alternatives, and results are expected to be the same.

3.4.1 EIS Spectrum Analyzer 1.0

This software has an extensive equivalent circuit model library, with 118 mathematical models selected from scientific publications and sorted by topics. Some categories are circuits used for batteries, fuel cells, semiconductors, solar cells, multilayers, and even a separate category for conducting polymers. The program enables user creation of new equivalent circuits by drawing them manually in the right section of the window. The main user interface is shown in Figure 8.

The input file format is a text document with three data columns, separated by spaces. The first column is the real part of the impedance, the second column is the inverse of the complex part of the impedance, and the third column is the frequency. Due to the specific order of the variables, a Python script was used to convert data from a FRI format (frequency, real, imaginary) to a RIF format (real, imaginary, frequency). The script is shown below.

```
1  import re   # regular expressions   -> for using re.sub()
2  import os   # operating system      -> for using os.walk()
3
4  for paths,dirs,files in os.walk('./data/'):
5      for file in files:                    # open all files recursively
6          f = open('./data/'+file,'r')        # open the current file (read)
7          content = f.readlines()             # returns a list with all lines
8          f.close()                           # closes the current file
9
10         size = len(content)
11         f = open('./data/'+file,'w')        # opens the current file (write)
12         f.write(str(size)+'\n')                 # first line: size of dataset
13
14         for i in range(0,size):
15             oldline = content[i]
16             line = re.sub(' +',' ',oldline[:-1])        # removes spaces and \n
17             space,freq,real,imag = line.split(' ')      # splits line in columns
18             f.write(real+' '+imag[1:]+' '+freq+'\n')    # new order of data
```

```
19
20          f.close()
```

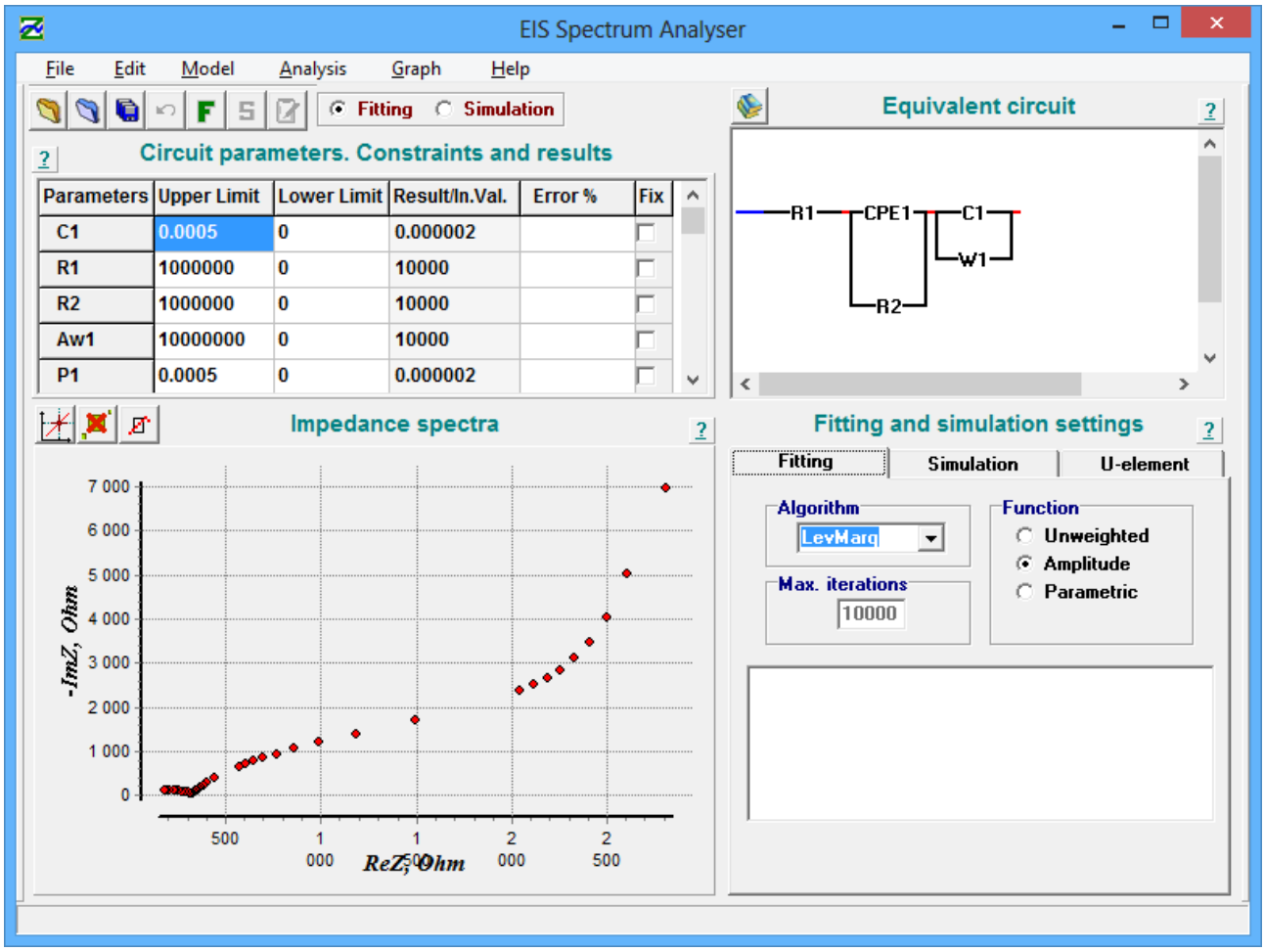

Figure 8: Graphical interface of the EIS Analyzer software.

This software was useful at the first stages of model exploration, because it includes a wide library of models, with references to indexed publications where the models were succesfully used. The models are grouped by category, materials, interfaces, and by number of lumped-parameter elements. This was the starting point to select a mathematical model to perform all the fittings.

One feature included with this program is the possibility of choosing the algorithm used to perform the fitting. There are four possible fitting algorithms: Nelder-Mead, Powell, Levenberg-Marquardt, and Newton.

However, this software does not include any possibility of initially guess the parameters for the fitting. This is important, because if the initial parameters are not set properly, convergence may not achieved, or it can be achieved with misleading values, providing irrelevant or incorrect information for the physical system in question. This was one of the reasons why this software was not used in the actual fitting section of this thesis.

3.4.2 James Ross Macdonald's LEVMW 8.12

J.R. Macdonald, Professor at the University of North Carolina, has been researching electrochemical impedance spectroscopy for many years, and he wrote the first book in this field in 1987 when this technique was just emerging. He wrote a computer program used to fit EIS experimental data to several models, applying numerical methods to extract passive elements from the curves. The program offers the possibility to choose from several pre-built circuit models, and enabling, disabling or replacing circuit elements to achieve the desired model. The current distribution of the software is the version 8.12 which runs on Microsoft Windows®. The main user interface is shown in Figure 9.

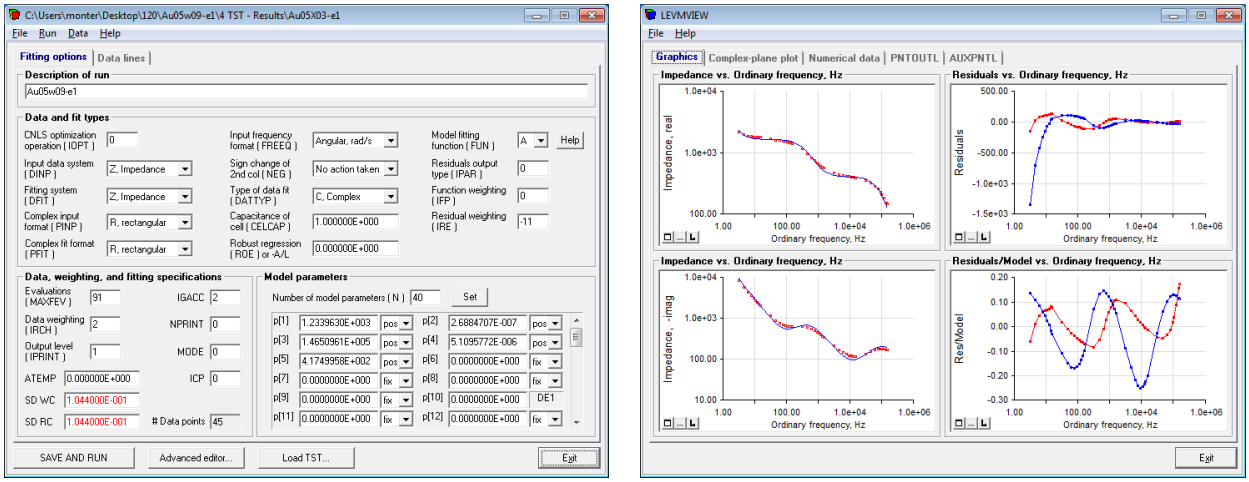

(a) Main interface of the LEVMW program. (b) Fitting results using the LEVMW program.

Figure 9: Graphical interface of the LEVMW fitting program written by James Ross Macdonald.

The program requires a specific file format for input data. The top part of the file is a header with information of the selected circuit, the initial conditions, and some configuration parameters regarding to the different options for the algorithm. The bottom part of the file contains three columns of data: the first one is the frequency, the second is the real part of the impedance, and the third column is the complex part of the impedance. Experimental data must be converted first from polar coordinates to rectangular coordinates, and arranged in this specific input format.

After preparing the required input file, the user can give initial values for the expected parameters of the model. The user can also set some parameters free while fixing others to a known value, or even force some parameters to have a positive value to preserve physical meaning of the model. Then the user can start the fit and observe the results of the fitting in a separate window. The program shows the input data in red, and the simulated Bode plot with the fitted parameters in blue. An example of this graphical interface is shown in Figure 9b.

However this toolbox has two main drawbacks. First, it is difficult to model different equivalent circuits found in the literature, because the available circuits are preconfigured and cannot be structurally changed. The only available option is to enable/disable circuit parameters. There is no way of creating new circuits, apart from the ones given in the user manual. And the second limitation is that the software can process only one input file at a time, consuming a lot of time to analyze the complete set of 96 samples for one single model.

3.4.3 Multiple EIS Parameterization (MEISP) 3.0

This software allows parallel processing of multiple input files. It also includes a schematic editor, enabling to draw the equivalent circuits from scratch. After drawing the circuits, the software can perform a DRC check (design rule check) to ensure that all the connections are valid, and then the software calculates a netlist, which is the mathematical representation of the model, used by the software to perform the fitting. The user interface of this software is displayed in Figure 10.

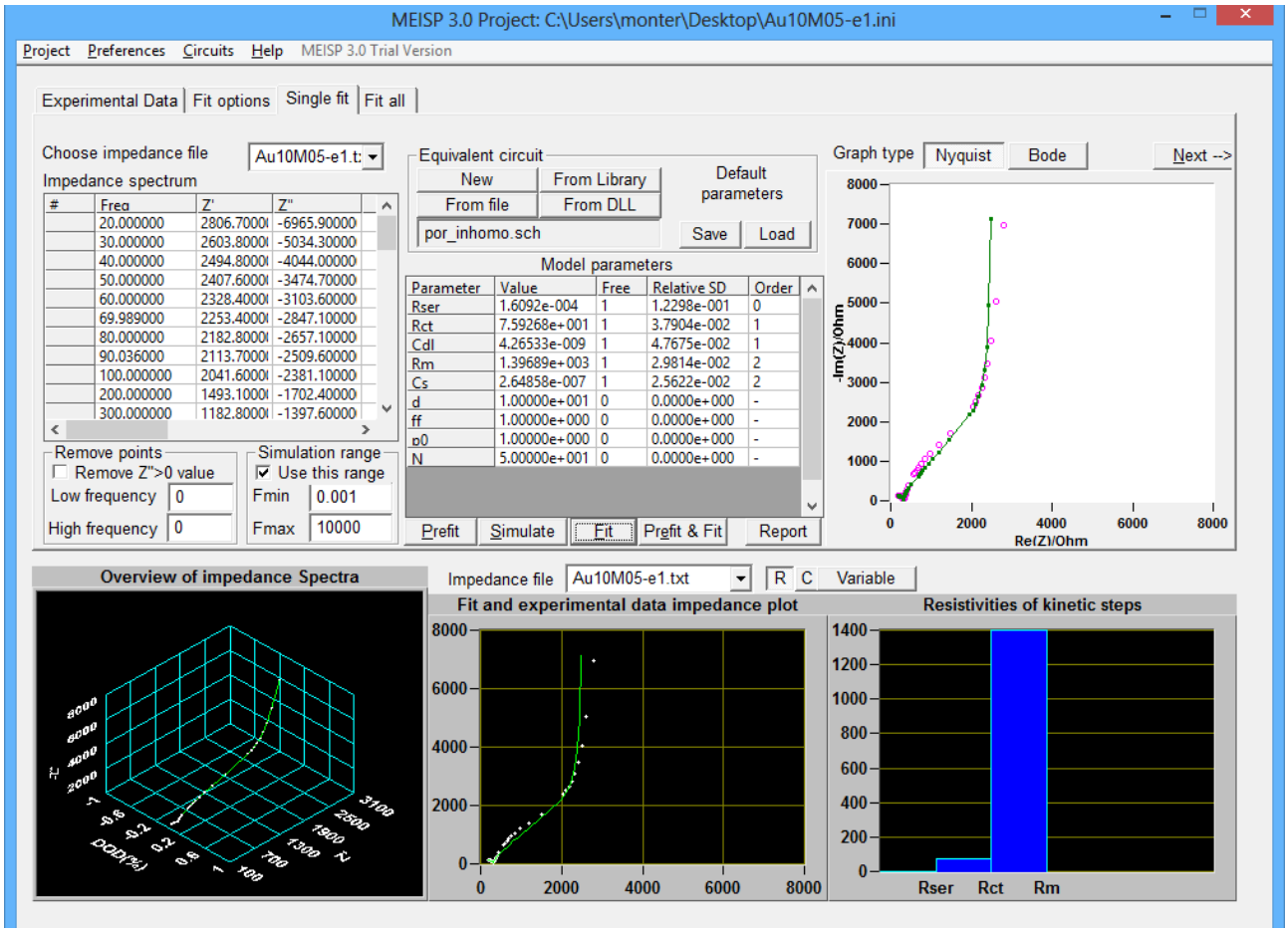

Figure 10: Graphical user interface of the MEISP 3.0 fitting program.

Another capability is the option to perform a pre-fit, eliminating the need for guessing the initial conditions manually, which can result in lack of convergence if the selected initial parameters are far from the final value.

The input data format is a conventional text document with experimental impedance data in rectangular coordinates, split in three columns, separated by spaces. This file format is simpler than J.R. Macdonald's format because it does not have a header.

The only limitation is that the program is currently discontinued: there is no commercial version available. However, there is a trial version that was freely distributed, and it is fully functional, without limitations on the calculations or any other of the software capabilities. A copy of the software can be retrieved from E. Barsoukov's collection of electrochemical impedance spectroscopy resources [14].

Chapter 4

Results

This chapter contains the detailed procedure to extract information from the experimental Bode and Nyquist plots of 96 electrode samples, characterized by Electrochemical Impedance Spectroscopy.

The first part of this chapter is a compilation of six mathematical models used by other researchers to describe polymeric and aqueous interfaces. We describe the standard double-layer model, the double-layer model with an additional geometrical capacitance, Macdonald's adsorption model, Voigt model, Bobacka's diffusion model, and Danielsson's expanded diffusive model. The first four equivalent circuit models were also simulated in MATLAB® to obtain the typical Bode and Nyquist diagrams. This section describes each model and associate their components with physical variables.

The second section describes the experimental data obtained previously by the research group at the TUHH, and explains the format preparations required to perform fittings using the CNLS program "LEVMW" provided by J.R. Macdonald. This format is also required by most of the available fitting software, which consists on a text file with three columns: frequency, real part of impedance, and imaginary part of impedance.

The third section of this chapter contains the fitting procedures and the results of these fitting processes, using the Complex Nonlinear Least Squares (CNLS) method. Numerical fitting was performed using two software tools: Macdonald's LEVMW, and MEISP 3.0. Both tools use internally the Levenberg-Marquardt algorithm for nonlinear fitting.

The fourth section of the chapter is a comparation of results from different models.

The fifth part of this chapter is the validation of Bobacka's model. This is achieved by applying linear regression to the bulk capacitance of the electrode, in order to extrapolate the capacitance values for two additional charge densities. Then, more electrode samples were fabricated using the same charge densities, to measure the EIS curves, fit the results and check if the fitted results were close to the predicted values.

4.1 Review of mathematical models

In this section we review six equivalent circuits used to model electrochemical systems, related with metallic, polymeric and aqueous media interfaces. The basic structure for all the equivalent models is the Randles cell, which is addressed first. Then we explain the double-layer model with and without geometrical capacitance, Macdonald's adsorption model [12], the Voigt cell structure [15] and the distributed models proposed by J. Bobacka [16] and P. Danielsson [17].

4.1.1 Randles Cell model

The Randles Cell explains the charge transfer process through a single interface [18]. This represents a metal electrode immersed in an aqueous solution, without any additional coating. The circuit components are the solution resistance (R1), the double-layer capacitance (C2) and the charge-transfer resistance (R2), as appreciated in Figure 11. The parallel combination of R2 and C2 is the simplest representation of an interface between two different materials, because the capacitor accounts for the charge accumulation at the interface, and the resistance stands for the conduction through this interface.

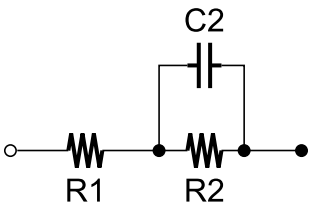

Figure 11: The Randles Cell Model.

The circuit was implemented in MATLAB® to appreciate its frequency response. The Bode and Nyquist plots are shown in Figure 12. The Bode plot features the response of a low-pass filter, and the final value of impedance (when the frequency tends to infinite) is the solution resistance, because the capacitance C2 is shorted at high frequencies. In the Nyquist diagram, this model produces a circle with two intercepts in the real axis. The intercept closest to the origin is the solution resistance, and the one farthest from the origin is the total cell resistance (R1 + R2).

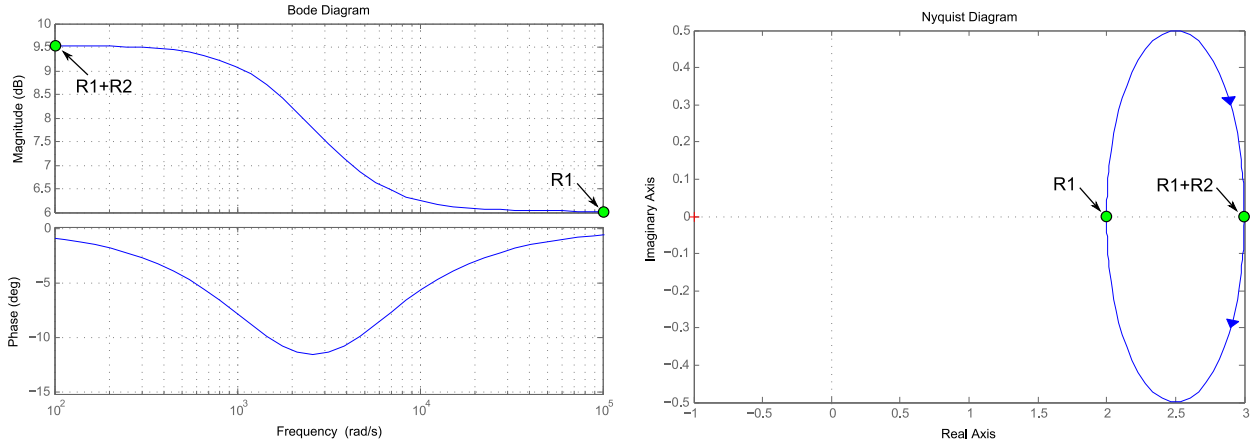

Figure 12: Simulation results of the Randles Cell.

MATLAB® simulations were implemented using scripts, applying the Laplace transform to calculate the impedance transfer function of the circuit, $Z(s)$, and using the *Control Systems Toolbox*™ to obtain the Bode and Nyquist plots of each model. For example, the MATLAB® script used to obtain the plots shown in Figure 12 is included below:

```
R1 = 2;
R2 = 1;
C = 0.00047;
w = logspace(1,5);  % Frequency range

% Bode Plot using the Control System Toolbox
% ------------------------------------------------------------------------
s = tf('s');
H = (R1 + (R2^-1 + (1/(s*C))^-1)^-1) ;

fig3 = figure(3);
bode(H)
grid on
set(fig3,'Position',[640 700 600 400]);

fig4 = figure(4);
nyquist(H)
set(fig4,'Position',[640 200 600 400]);

% Bode Plots manually
% ------------------------------------------------------------------------
Zmag = abs( (R1 + (R2^-1 + (1./(1i*w*C)).^-1).^-1) );
Zphase = angle( (R1 + (R2^-1 + (1./(1i*w*C)).^-1).^-1) ) * 360 / (2 * pi);

% Magnitude Plot
    fig5 = figure(5);
    semilogx(w,Zmag,'linewidth',3,'color',[0 0 0.8]);
    grid on
    title('Bode Plot: Magnitude');
    xlabel('Frequency [Hz]');
    ylabel('Impedance [\Omega]');
    set(fig5,'Position',[20 700 600 400]);

% Phase Plot
    fig6 = figure(6);
    semilogx(w,Zphase,'linewidth',3,'color',[0.8 0 0]);
    grid on
    title('Bode Plot: Phase');
    xlabel('Frequency [Hz]');
    ylabel('Phase [°]');
    set(fig6,'Position',[20 200 600 400]);

```

4.1.2 Double Layer Model

This model is an extension of the Randles cell, because it involves two interfaces instead of one. It was the first model used for the fittings in this master's thesis, because it includes the electrode/polymer interface and the polymer/electrolyte interface. Each interface is represented by an RC parallel circuit, where the resistive element explains the charge transfer through the interface, and the capacitive element is related with charge accumulation at that interface.

The double-layer model can be represented schematically in our experimental configuration as can be seen in Figure 13. The leftmost part of the circuit is the gold electrode, which also known as the working electrode in an EIS experiment. This electrode is coated with a uniform layer of polymer, and the thickness of this layer is determined by the charge density applied at polymerization time. Then the polymer is in direct contact with the solution, and the rightmost part of this picture is the reference electrode, which is the container of the solution, and it is connected to ground.

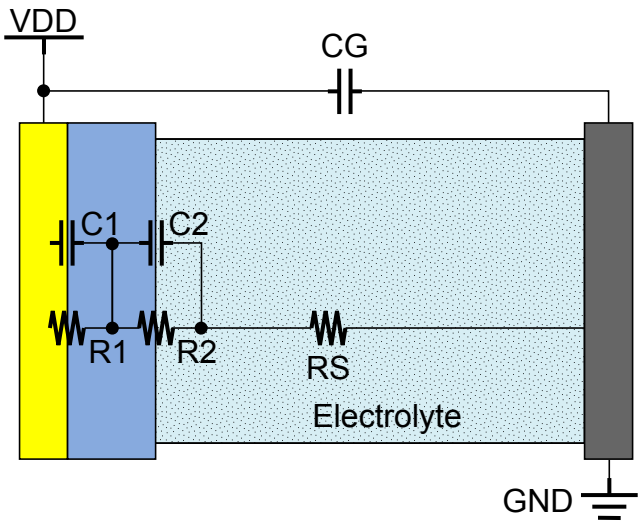

Figure 13: Equivalent circuit elements involved in the experiment.

The capacitor labeled as C_G is the geometrical capacitance, and it is often ommited because its value is small. I have used the model ommitting it (referenced as the double-layer model), and also including it (referenced as the double-layer with CG), and fittings were achieved for both models in the results section.

The schematic representation for the double-layer model with CG is shown in Figure 14.

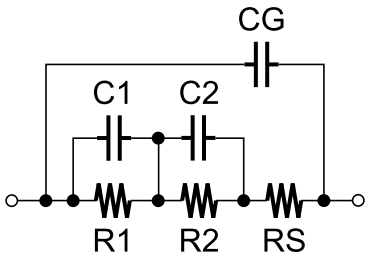

Figure 14: The Double-Layer Model with geometrical capacitance.

The detailed explanation of each component is as follows:

- C_G is the geometrical capacitance, and it depends on the placement of the working electrode respect to the reference electrode, as well to the dielectric constant of the solution.
- R_S is the solution resistance, and it depends also on the electrode placement.
- C_1 is the contact capacitance, related with the accumulation of charge between the metal and the polymer.
- R_1 is the contact resistance, and it depends on the electrical contact between the metal and the polymer, as well as the electrical resistance of the polymer itself.
- C_2 is the double-layer capacitance, due to dipole interactions in the solution near the electrode surface.
- R_2 is the reaction resistance, and depends on the charge transfer between the electronic conduction region (metal) and the ionic conduction region (solution).

The circuit was implemented in MATLAB® to appreciate its frequency response. The Bode and Nyquist plots are shown in Figure 15. The Bode plot features the response of a low-pass filter, and the final value of impedance (when the frequency tends to infinite) is the solution resistance, because the capacitances C1 and C2 are shorted at high frequencies. It also should be noticed that the phase plot ends with a phase shift that tends to zero, but this is not always equal for all the models (see Macdonalds model in the following section). In the Nyquist diagram, this model produces two semicircles, one for each RC parallel combination. There are two intercepts in the real axis. The intercept closest to the origin is the solution resistance, and the one farthest from the origin is the total cell resistance (R1 + R2 + R3).

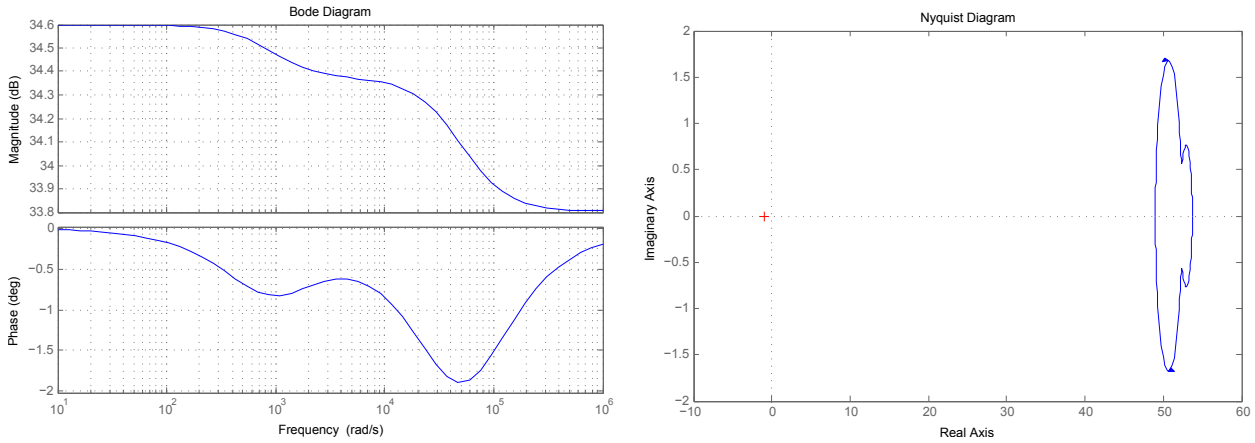

Figure 15: Simulation results of the Double-Layer model.

4.1.3 Macdonald's Model

J.R. Macdonald has proposed an equivalent circuit used to fit EIS data for binary electrolytes (electrolytes that dissociate reversibly into two ions of different charge) [12]. The model is applicable for liquid electrolytes such as the NaCl solution used in our experimental setup, and also for solid electrolytes like glass or crystals.

The model considers an electrochemical reaction at the electrode surface, where ions are adsorbed at the surroundings of the interface, forming a double-layer of charge in the aqueous solution. The equivalent circuit is shown in Figure 16.

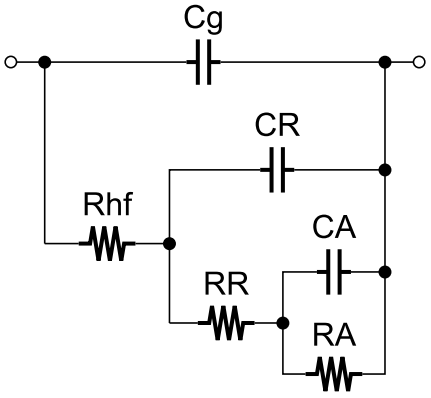

Figure 16: The model proposed by J.R. Macdonald.

The included circuit elements are the geometrical capacitance (Cg), high-frequency limiting resistance (Rhf), double-layer capacitance (CR), reaction resistance (RR), adsorption resistance (RA) and adsorption capacitance (CA). Some of these parameters are mathematically equivalent to the elements present in the double-layer model with geometrical capacitance, because both models contain three resistors and three capacitors, and are of the same degree. For example, the high-frequency limiting resistance can be obtained directly from the Bode plot (when frequency tends to infinity), because it is equivalent to the solution resistance from the double-layer model.

A MATLAB® simulation with arbitrary parameters is shown in Figure 17.

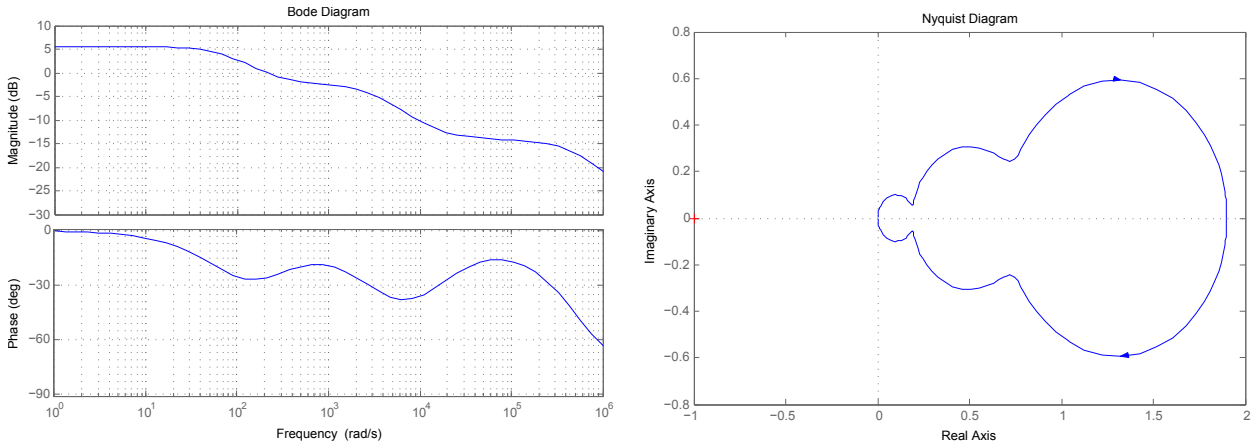

Figure 17: Simulation results of the RC series circuit.

4.1.4 Voigt Model with three RC elements

The Voigt model can be described as an expansion of the double-layer model **??**, because it contains one additional RC combination. It allows a further division of the interfaces and electrochemical processes in the electrode.

The first RC element describes the metal/polymer interface, the second RC combination describes the polymer/aqueous interface, and the third RC parallel combination is related to the double-layer present in the electrolyte solution. Finally the resistive element stands for the solution resistance.

Theoretically, a Voigt model can be built using any number of RC parallel cells, connected in series. However, for more than three cells, this circuit loses its geometrical significance for the experimental setup that we are using. With three RC combinations we describe both interfaces and the double-layer effect in the surroundings of the electrode: an additional fourth RC combination would not have any physical significance.

The equivalent circuit is shown in Figure 18.

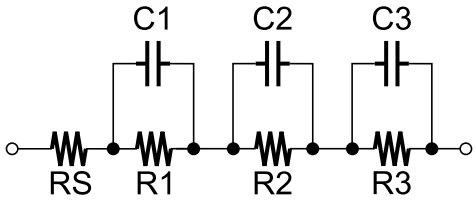

Figure 18: Voigt model with three RC elements in series [7].

The frequency response of this model features three semicircles in the Nyquist diagram, one for each RC parallel combination. It is useful for fitting and adjusting a wide range of experimental conditions, because RC elements can be shorted or removed depending on the experimental situation, and the position of the semicircles can be precisely adjusted by selecting the proper time constants for each RC pair. The three semicircles of the Nyquist diagram, with the corresponding Bode plots, can be appreciated in the MATLAB® simulation of Figure 19.

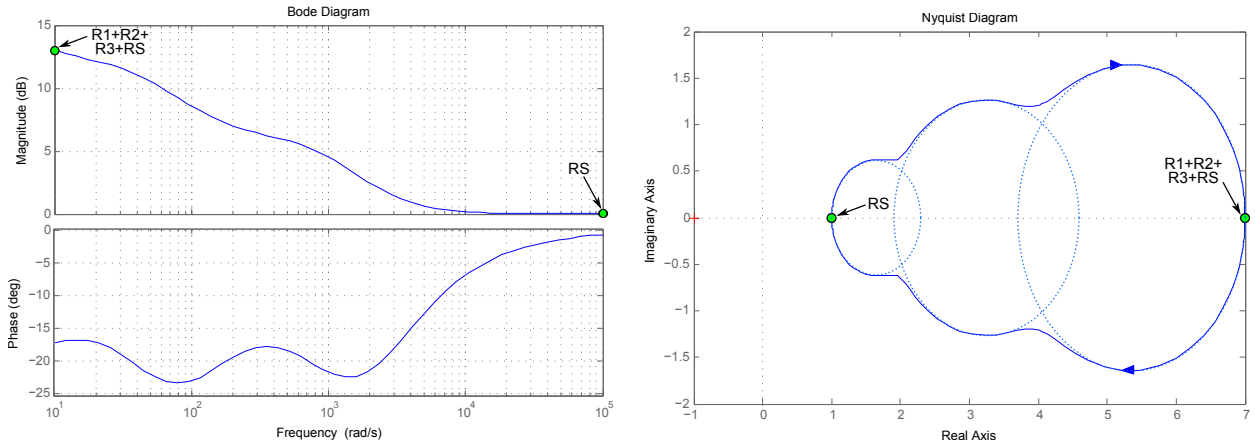

Figure 19: Simulation results of the Voigt model with three RC elements.

4.1.5 Bobacka's diffusion model

Until now, all the studied models are based on electrical components that are ideal, for example capacitances, resistances and inductances that are localized in one point of space. But this is not true in real systems, because each part of the electrochemical system is extended over a finite region of space. The response of an input stimulus can be delayed while propagated across the whole system, in a behavior similar to an electrical transmission line. In an aqueous solution, conductivity is not as high as in metals, because ions move slowly and these propagation effects are increased. This is the reason why distributed elements are required in mathematical modeling: they reproduce propagation through spatially-distributed elements in a more accurate way.

The simplest model to describe a PEDOT/aqueous interface, considering propagation effects, was studied by J. Bobacka *et al.* [8]. He built a similar PEDOT electrode in contact with an aqueous solution. The polymer was doped with poly (sodium 4-styrenesulfonate) (NaPSS) and other supporting electrolytes. The only difference with our experimental setup is that they applied a DC-bias of 2 V to permanently oxidize the polymer, and then applied a small-signal AC variation to study the frequency response. We do not have this offset in our system, but the results are expected to be similar. The mathematical model used by this research group is shown in Figure 20.

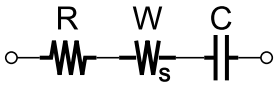

Figure 20: Diffusion model with Warburg element.

Each component can be related with a physical parameter: the resistance R represents the charge transfer process in the electrolyte, and it is called the solution resistance. The finite-length Warburg element is the equivalent of a shorted transmission line, and explains the diffusive charge transfer in the polymer coating. And the capacitor describes charge accumulation at the interface between polymer/aqueous media. This model can be expanded as shown in Figure 21.

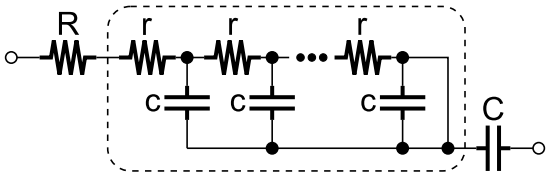

Figure 21: Diffusion model with Warburg element (expanded).

The choice between a short-circuit Warburg element and an open-circuit Warburg depends on the charge transfer mechanism. The shorted element is also known as a transmissive finite-length diffusion, and the open-circuit element is known as a reflective finite-length diffusion, which means that in the first case the ions are flowing from the polymer to the aqueous media, as through a porous membrane (the structure of the PEDOT), and in the second case the ions are blocked by this equivalent membrane and cannot pass through it. The shorted-circuit element was used here because ions can move from the polymer to the solution.

4.1.6 Danielsson's extension to Bobacka's model

Bobacka's model is a phyisical representation of the distributed metal/aqueous interface, but it does not describe the double-layer charge accumulation at the electrolyte. To account the effects of ion accumulation in the surroundings of the electrode, an additional RC parallel combination is added to Bobacka's model, as described by P. Danielsson [17].

The resistance R_{ct} describes the charge transfer at the polymer/aqueous interface, and the capacitance C_{dl} stands for the double-layer charge accumulation. The equivalent model is shown in Figure 22.

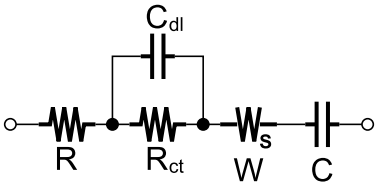

Figure 22: Extended diffusion model with Warburg element.

The Warburg element can be expanded in the same way as for Bobacka's model. The expanded equivalent cicuit is shown in Figure 23. Again, the model can include the open-circuit Warburg element (W_o) for a blocked electrode where charge cannot flow through the electrode, or the short-circuit Warburg element (W_s) for a conductive electrode where charge is transferred efficiently. Here we are using the shorted-circuit version, because the Bode and Nyquist plots suggest low resistivities for a wide range of frequencies.

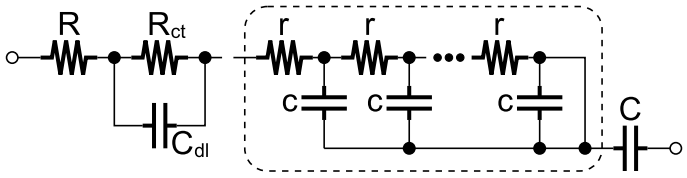

Figure 23: Extended diffusion model with Warburg element (expanded).

We have explained the six mathematical models selected to perform fittings in this master's thesis: the standard double-layer model, the double-layer model with geometrical capacitance, Macdonald's binary electrolyte model, Voigt's model with three RC parallel combinations, Bobacka's ion diffusion model, and Danielsson's expansion for a double interface system.

In the next sections of this thesis we are going to analyze the original data obtained from the experimental setup, and use it to perform the fitting for these six mathematiacal models. Then we look for trends in some important parameters such as the solution resistance and the capacitances of the metal/polymer and polymer/solution interfaces, and compare the fittings achieved with different models.

4.2 Source data formatting

Experimental data for 12 samples of 8 electrodes each (96 independent electrodes in total) had been obtained previously by researchers at the TUHH, and it is stored in MATLAB® files. The complete set of available data is plotted in MATLAB® and displayed in Figure 24.

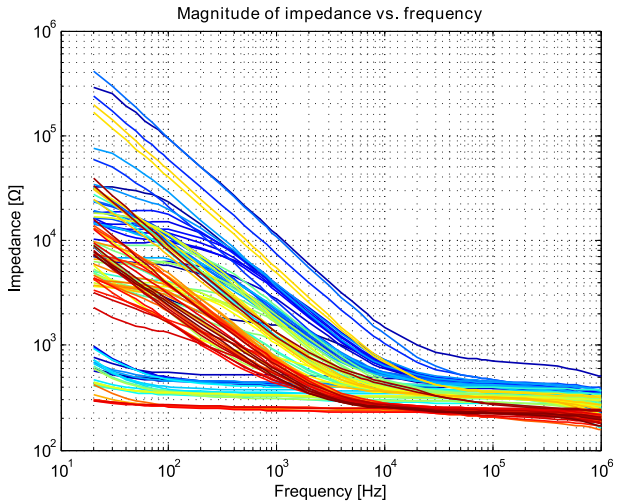

(a) Magnitude of impedance vs. frequency.

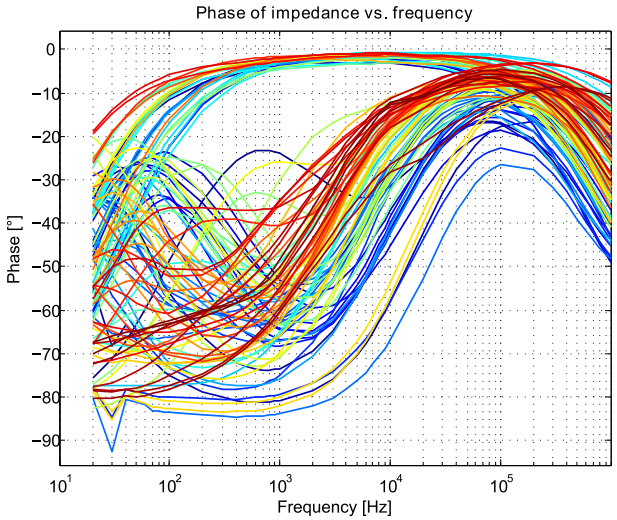

(b) Phase of impedance vs. frequency.

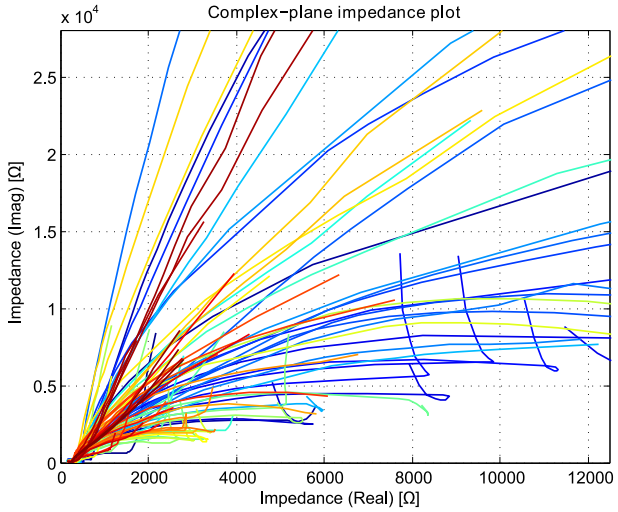

(c) Complex-plane plot (Nyquist).

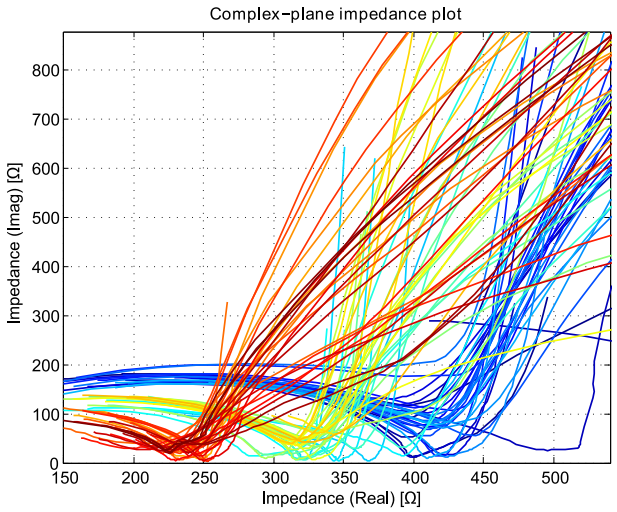

(d) Complex-plane plot (zoomed).

Figure 24: Bode and Nyquist plots of all the experimental data.

There are two fabrication parameters that were adjusted at the polymerization time: the surface area of the electrode, and the charge density, which is proportional to the polymer thickness. By adjusting these parameters independently, we can observe the effect of them in the overall electrical performance of the electrode. A mathematical model can be used to optimize the fabrication process, and it could be used to predict the electrode behavior for different experimental conditions, before fabricating the actual electrodes.

The **surface area** (A) is constant for the eight electrodes in each sample. There are four samples (32 individual electrodes) with an electrode surface area of 0,5 mm^2, four samples of 1,0 mm^2 and four samples of 2,0 mm^2.

The **charge density** (CD) at deposition time can be adjusted individually for each electrode, and it determines the thickness of the polymeric coating. We have experimental data for electrodes with a charge density of 40 mC/cm^2, 80 mC/cm^2, 120 mC/cm^2, and also for uncoated gold electrodes which are used as reference, labeled with a charge density of 0 mC/cm^2.

There are three groups of curves in plot (d) from Figure 24, each one related with the surface area of the electrodes. We have experimental data for electrodes of 0,5 mm^2; 1,0 mm^2 and 2,0 mm^2. The lowest point in all these curves of plot (d) is the solution resistance, and it is inversely proportional to the surface area.

During the development of this master's thesis, we also obtained experimental data for a single sample (eight individual electrodes) with a surface area of 1,0 mm^2. In this additional sample, there are three electrodes with CD of 20 mC/cm^2, three electrodes with CD of 60 mC/cm^2, one electrode with an arbitrary value of CD (unknown because the deposition time was not measured at the time of the polymerization) and one reference electrode.

Source data had to be prepared and exported from MATLAB® to a compatible format for the LEVM and MEISP software. These tools required the input data in rectangular coordinates, with a three-column array of data. The first column is required to be the frequency of the input signal; the second column is the real part of the impedance; and the third column is the complex part of the impedance. Since we had the data in polar coordinates, and was stored in a binary .mat file, a MATLAB® script was required to export all data to a standard text file, separated by spaces.

The script used to export a single sample of eight electrodes is shown here:

```
load('C:\Users\monter\Documents\MATLAB\DATA\Au20T01.mat')

% Express impedance in rectangular coordinates -----------------------------
Zreal1 = Ze1 .* cos(phasee1 * pi / 180);
Zreal2 = Ze2 .* cos(phasee2 * pi / 180);
Zreal3 = Ze3 .* cos(phasee3 * pi / 180);
Zreal4 = Ze4 .* cos(phasee4 * pi / 180);
Zreal5 = Ze5 .* cos(phasee5 * pi / 180);
Zreal6 = Ze6 .* cos(phasee6 * pi / 180);
Zreal7 = Ze7 .* cos(phasee7 * pi / 180);
Zreal8 = Ze8 .* cos(phasee8 * pi / 180);
Zimag1 = Ze1 .* sin(phasee1 * pi / 180);
Zimag2 = Ze2 .* sin(phasee2 * pi / 180);
Zimag3 = Ze3 .* sin(phasee3 * pi / 180);
Zimag4 = Ze4 .* sin(phasee4 * pi / 180);
Zimag5 = Ze5 .* sin(phasee5 * pi / 180);
Zimag6 = Ze6 .* sin(phasee6 * pi / 180);
Zimag7 = Ze7 .* sin(phasee7 * pi / 180);
Zimag8 = Ze8 .* sin(phasee8 * pi / 180);

% Convert row vectors into column vectors ----------------------------------
frequenz = transpose(frequenz);
Zreal1 = transpose(Zreal1);
Zreal2 = transpose(Zreal2);
Zreal3 = transpose(Zreal3);
Zreal4 = transpose(Zreal4);
Zreal5 = transpose(Zreal5);
Zreal6 = transpose(Zreal6);
Zreal7 = transpose(Zreal7);
Zreal8 = transpose(Zreal8);
Zimag1 = transpose(Zimag1);
```

```
Zimag2 = transpose(Zimag2);
Zimag3 = transpose(Zimag3);
Zimag4 = transpose(Zimag4);
Zimag5 = transpose(Zimag5);
Zimag6 = transpose(Zimag6);
Zimag7 = transpose(Zimag7);
Zimag8 = transpose(Zimag8);

% Write the rectangular coordinate vectors in INTRAN ----------------------
dlmwrite('INTRAN1',[frequenz Zreal1 Zimag1],' ');
dlmwrite('INTRAN2',[frequenz Zreal2 Zimag2],' ');
dlmwrite('INTRAN3',[frequenz Zreal3 Zimag3],' ');
dlmwrite('INTRAN4',[frequenz Zreal4 Zimag4],' ');
dlmwrite('INTRAN5',[frequenz Zreal5 Zimag5],' ');
dlmwrite('INTRAN6',[frequenz Zreal6 Zimag6],' ');
dlmwrite('INTRAN7',[frequenz Zreal7 Zimag7],' ');
dlmwrite('INTRAN8',[frequenz Zreal8 Zimag8],' ');
```

After exporting the data to independent text files, the number of decimals has to be standarized using a program called DINPUT.EXE, included with Macdonald's LEVMW software. The results are stored in an OUTRAN file.

Macdonald's LEVMW data files also require a header, specifying the fitting circuit, initial conditions and configuration parameters of the tool. The header is added with the graphical interface of the software, selecting a template for the desired circuit and then loading the data from the OUTRAN file. An example of an input file with the proper format is shown below:

```
Au10R03-e1
   0  ZZRR  A .1000D+01C         0 .0000D+00     0   -11
   45   40  900    0    2    0    0    1    2 .0000D+00   .1098D+00   .1098D+00
  .10630146D+06  .48337392D-05  .14025912D+03  .77151128D-06  .31116777D+03
  .00000000D+00  .00000000D+00  .00000000D+00  .00000000D+00  .00000000D+00
  .00000000D+00  .00000000D+00  .00000000D+00  .00000000D+00  .00000000D+00
  .00000000D+00  .00000000D+00  .00000000D+00  .00000000D+00  .00000000D+00
  .00000000D+00  .00000000D+00  .00000000D+00  .00000000D+00  .00000000D+00
  .00000000D+00  .00000000D+00  .00000000D+00  .35251748D-08  .00000000D+00
  .00000000D+00  .10000000D+01  .00000000D+00  .00000000D+00  .00000000D+00
  .00000000D+00  .00000000D+00  .00000000D+00  .00000000D+00  .00000000D+00
1111100000000000000000000000100000000000
    1       .2000000000000D+02       .1147600000000D+04      -.8925400000000D+04
    2       .3000000000000D+02       .9157000000000D+03      -.6084300000000D+04
    3       .4000000000000D+02       .8282000000000D+03      -.4654500000000D+04
    4       .5000000000000D+02       .7633500000000D+03      -.3790200000000D+04
    5       .6000000000000D+02       .7207300000000D+03      -.3205200000000D+04
    6       .6998900000000D+02       .6874100000000D+03      -.2797500000000D+04
    7       .8000000000000D+02       .6615600000000D+03      -.2474400000000D+04
    8       .9003600000000D+02       .6437600000000D+03      -.2222600000000D+04
    9       .1000000000000D+03       .6278600000000D+03      -.2016700000000D+04
   10       .2000000000000D+03       .5442900000000D+03      -.1061100000000D+04
   11       .3000000000000D+03       .5109500000000D+03      -.7358400000000D+03
   12       .4000000000000D+03       .4934700000000D+03      -.5685200000000D+03
   13       .5000000000000D+03       .4823400000000D+03      -.4669700000000D+03
   14       .6000000000000D+03       .4739100000000D+03      -.3985000000000D+03
   15       .7009300000000D+03       .4676000000000D+03      -.3492200000000D+03
   16       .8000000000000D+03       .4630100000000D+03      -.3128300000000D+03
   17       .9036100000000D+03       .4591100000000D+03      -.2833500000000D+03
   18       .1000000000000D+04       .4552300000000D+03      -.2611000000000D+03
```

```
19      .2000000000000D+04      .4328700000000D+03      -.1581700000000D+03
20      .3000000000000D+04      .4196000000000D+03      -.1262200000000D+03
21      .4000000000000D+04      .4089200000000D+03      -.1113400000000D+03
22      .5000000000000D+04      .3994200000000D+03      -.1024800000000D+03
23      .6000000000000D+04      .3910600000000D+03      -.9638500000000D+02
24      .6944400000000D+04      .3844000000000D+03      -.9179200000000D+02
25      .8000000000000D+04      .3775700000000D+03      -.8733200000000D+02
26      .8928600000000D+04      .3726800000000D+03      -.8396400000000D+02
27      .1000000000000D+05      .3675800000000D+03      -.8056900000000D+02
28      .2000000000000D+05      .3425000000000D+03      -.6261200000000D+02
29      .3000000000000D+05      .3309900000000D+03      -.5438900000000D+02
30      .4000000000000D+05      .3248300000000D+03      -.5075400000000D+02
31      .5000000000000D+05      .3207600000000D+03      -.4941300000000D+02
32      .6000000000000D+05      .3176600000000D+03      -.4935400000000D+02
33      .7142900000000D+05      .3148800000000D+03      -.5016500000000D+02
34      .8000000000000D+05      .3129200000000D+03      -.5121600000000D+02
35      .8571400000000D+05      .3117400000000D+03      -.5208000000000D+02
36      .1000000000000D+06      .3087500000000D+03      -.5451400000000D+02
37      .2000000000000D+06      .2905400000000D+03      -.7571000000000D+02
38      .3000000000000D+06      .2707800000000D+03      -.9519000000000D+02
39      .4000000000000D+06      .2502100000000D+03      -.1098100000000D+03
40      .5000000000000D+06      .2299900000000D+03      -.1199300000000D+03
41      .6000000000000D+06      .2106600000000D+03      -.1264500000000D+03
42      .6666700000000D+06      .1987900000000D+03      -.1290500000000D+03
43      .8000000000000D+06      .1770700000000D+03      -.1312900000000D+03
44      .9600000000000D+06      .1550300000000D+03      -.1303900000000D+03
45      .1000000000000D+07      .1501500000000D+03      -.1298000000000D+03
```

The input files are prepared manually, one by one, first loading the desired circuit from a template (TMP) header, and then loading the pre-processed OUTRAN file. The complete input file with header and data is then save in a TST file. This is a time-consuming task, and the whole set of 96 data files is useful only for one model. To select a different model, each header in the individual TST data file has to be replaced with a new header, specifying the new equivalent circuit by loading a new TMP header, and reloading the data from the OUTRAN file.

The overall data flow can be appreciated in Figure 25. This diagram shows each file used to perform a complete fitting of a single MATLAB® file, containing eight independent electrodes. This has to be repeated for the whole set of 12 samples, and twice to be able to use two models: the double-layer model and Macdonald's binary electrolyte model. There are 192 TST files containing the original Bode/Nyquist information and the fitting results.

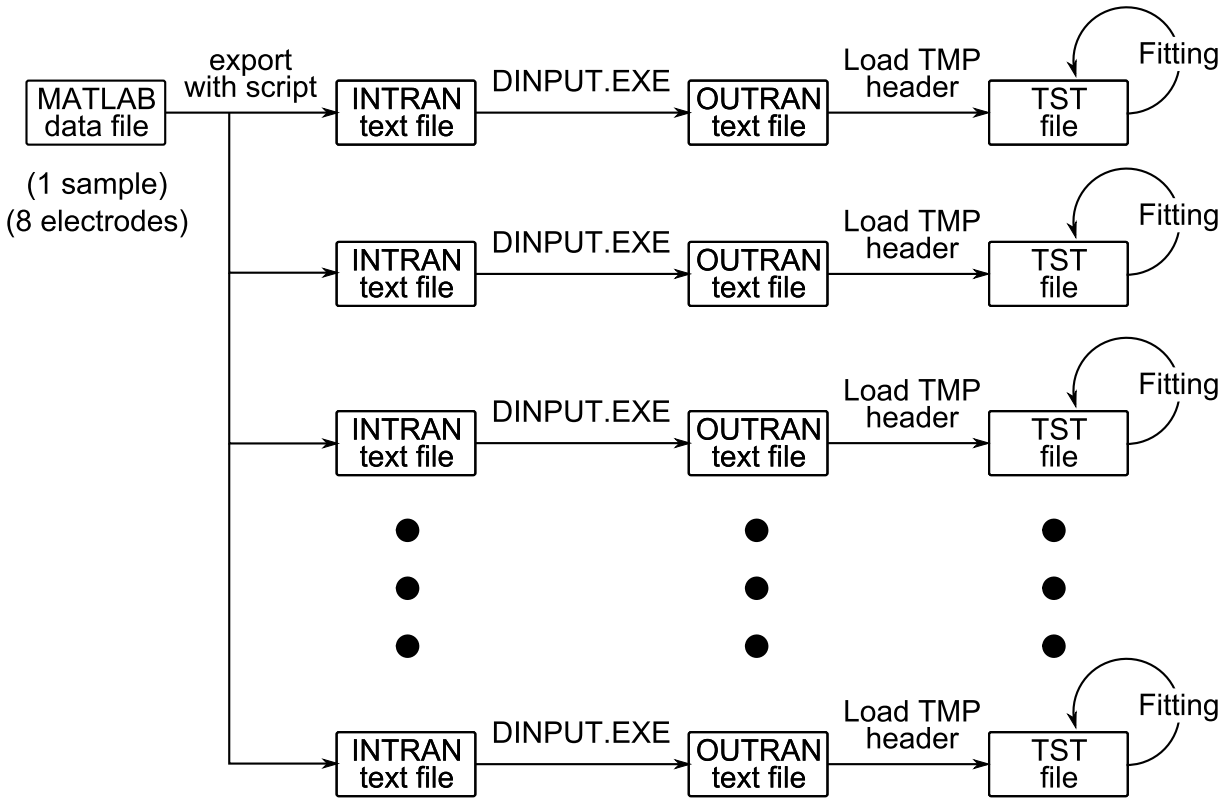

Figure 25: Data flow for simulations in Macdonald's LEVMW.

4.3 Model fitting

Experimental data was fitted to the six equivalent circuit models described in the previous section, using numerical fitting software.

The first program used to perform the calculations is J.R. Macdonald's LEVMW 8.12 which enables to perform fittings to predefined circuits. It included options to make the fitting to all the required models, but the fitting process is time-consuming because it does not have parallel data processing capabilities. The user needs to give an input file, adjust all the preliminary parameters and fit to obtain results, and then repeat for the entire set of data.

The second fitting program is the MEISP 3.0 software, which uses the same Levenberg-Marquardt algorithm in the background, and the achieved results are exactly the same. This software enables to add many input files at once, for parallel processing of all of them at the same time. Also this software includes a pre-fitter, so it can automatically guess the initial conditions of the parameters, eliminating the need of setting them manually.

4.3.1 Double-layer model fitting

To do the fitting using Macdonald's LEVMW, the user needs to select one of the predefined equivalent circuits included in the software, and customize it, enabling or disabling parameters to get the desired model. The complete list of models and the details of them are included in the manual of the software, with an explanation of every parameter. Models are labeled with a letter from A to O, and there are some extra letters for different special purposes.

For the implementation of the double-layer model, the selected equivalent circuit was the circuit A, which can be observed in Figure 26. As it can be seen, the model has many parameters, and for a double-layer model we would like to eliminate some of them, leaving only the basic structure of two capacitors and three resistances, with the additional geometrical capacitance.

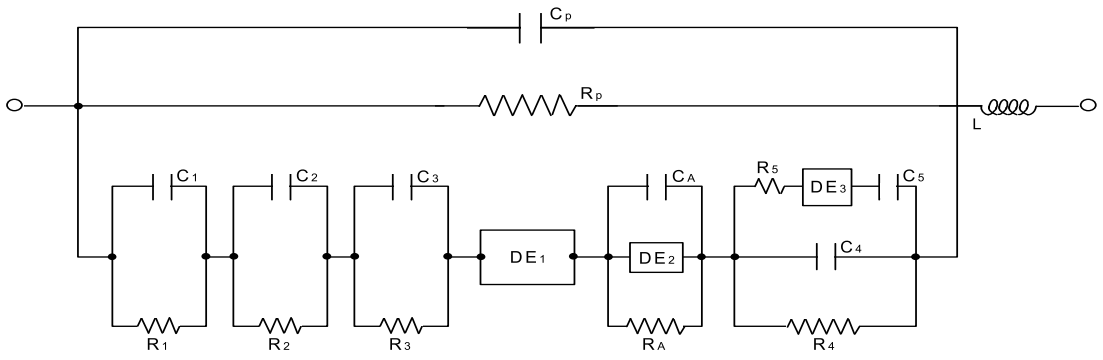

Figure 26: Pre-defined circuit A, included in the LEVMW manual.

The complete parameter association for this circuit is detailed in Table 4.1. Each "P" parameter can be accessed directly in the software graphical interface, and can be fixed to a constant value in case it is known, or can be set to zero to remove the element completely from the circuit, or also can be set free for numerical approximation by the Levenberg- Marquardt algorithm.

Table 4.1: Parameter association for circuit A in the LEVMW software.

Element	Label		Element	Label		Element	Label
R1	P(1)		RDE2	P(11)		C3	P(21)
C1	P(2)		TDE2	P(12)		RA	P(22)
R2	P(3)		UDE2	P(13)		CA	P(23)
C2	P(4)		PDE2	P(14)		R4	P(24)
R3	P(5)		NDE2	P(15)		C4	P(25)
RDE1	P(6)		RDE3	P(16)		R5	P(26)
TDE1	P(7)		TDE3	P(17)		C5	P(27)
UDE1	P(8)		UDE3	P(18)		RP	P(28)
PDE1	P(9)		PDE3	P(19)		CP	P(29)
NDE1	P(10)		NDE3	P(20)		L	P(30)

In this case, parameters P(1) to P(5) were set free with a positive value restriction, and this is also applied for the P(29) parameter. The rest of the elements were set to zero in order to discard them from the system. The resulting equivalent circuit when using these settings is the double-layer model with an extra capacitor, observed in Figure 14.

Results are observed in Figure 27.

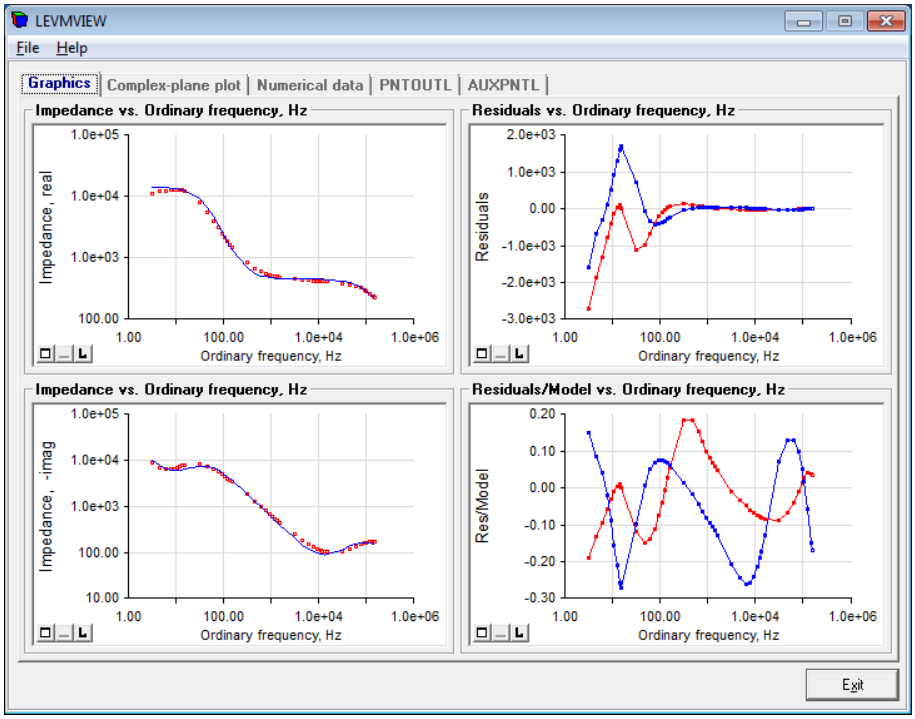

Figure 27: Fitting results for file 05/40/Au05X03-e3.mat. Red: source data. Blue: fitted data.

Graphical results for this model can be appreciated in Figure 28. The plots below represent the data for an electrode with surface area of 1,0 mm^2, although the same fitting was performed for electrodes of 0,5 mm^2 and 2,0 mm^2.

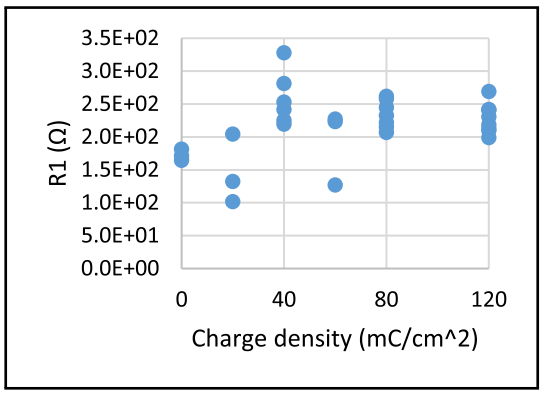

(a) Metal/polymer resistance.

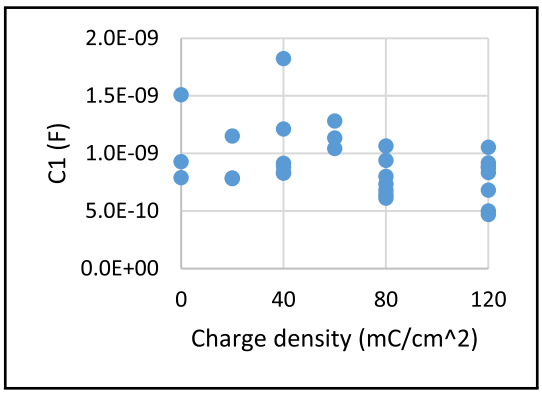

(b) Metal/polymer capacitance.

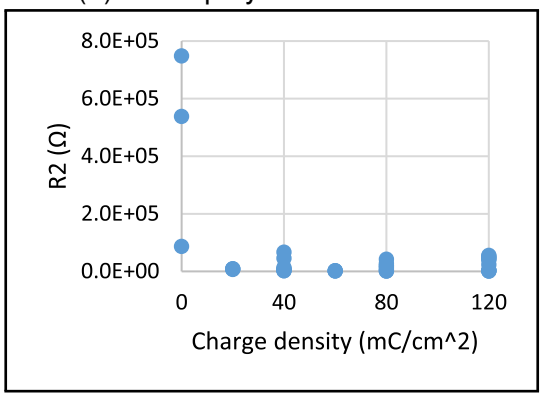

(c) Polymer/solution resistance.

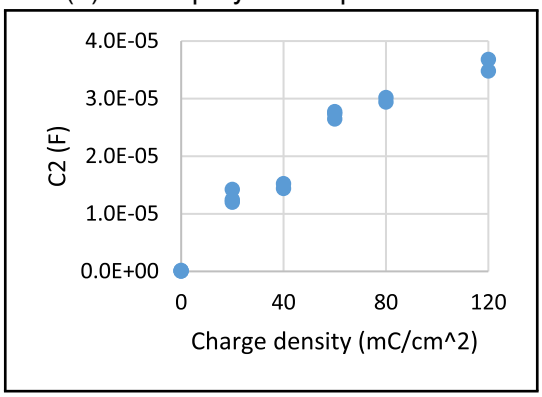

(d) Polymer/solution capacitance.

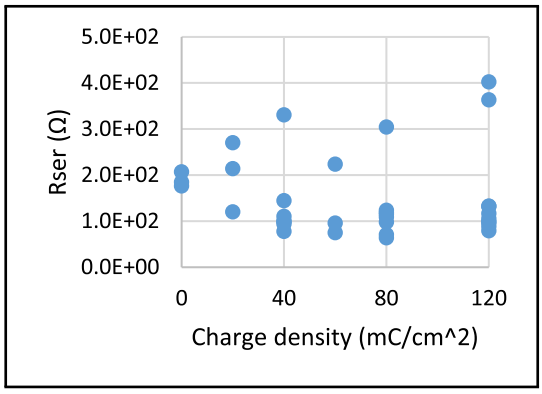

(e) Series resistance.

Figure 28: Fitting results for the double-layer model.

As can be seen from these plots, capacitance in the overall electrode is dominated by the polymer/solution capacitance shown in (d), because it is four orders of magnitude higher than the capacitance between metal/polymer shown in (b). This was in accordance with the experimental results from J. Bobacka *et al.* [16].

As expected, capacitances in this model increase linearly with the charge density at deposition time: higher charge densities result in thicker polymer layers, and charge is accumulated in bulkier polymeric coatings.

If the geometrical capacitance is considered, then the results can be observed in Figure 29.

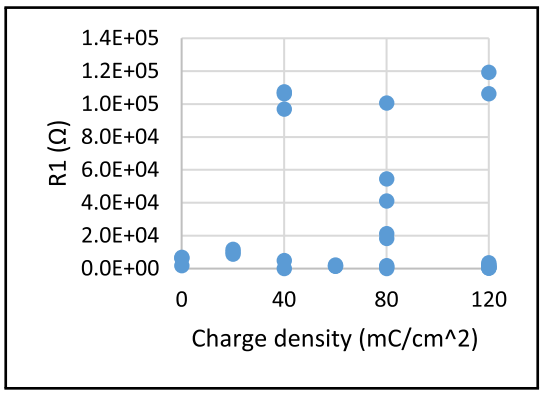

(a) Metal/polymer resistance.

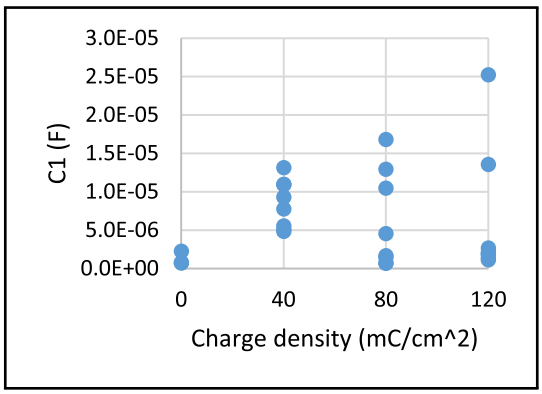

(b) Metal/polymer capacitance.

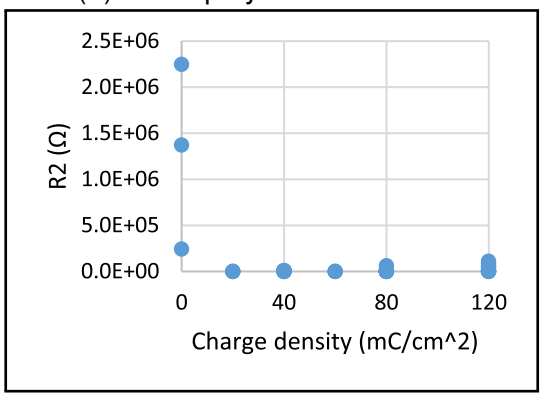

(c) Polymer/solution resistance.

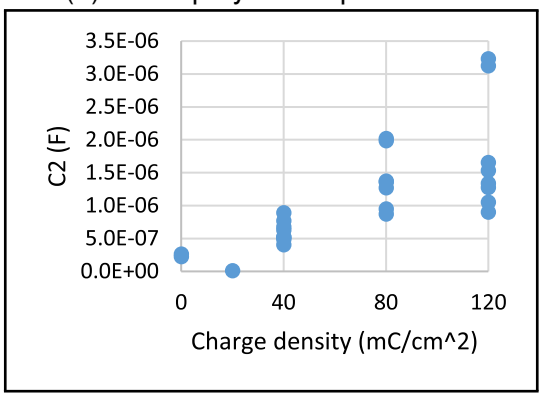

(d) Polymer/solution capacitance.

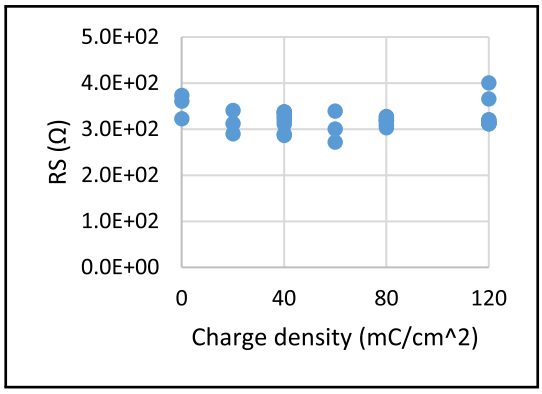

(e) Series resistance.

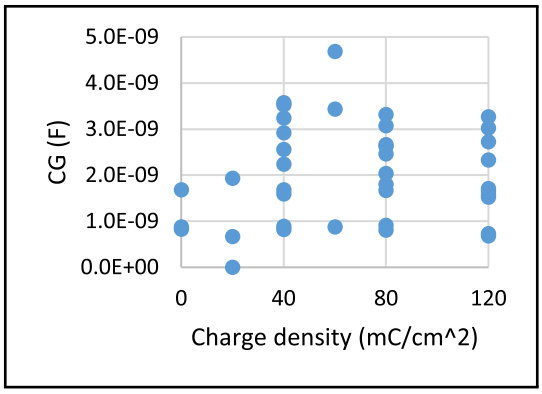

(f) Geometrical capacitance.

Figure 29: Fitting results for the double-layer model with geometrical capacitance.

This second fitting, considering the geometrical capacitance, improves the extraction of the solution resistance, which now is consistent with the expected values seen in the Bode plots from Figure 24. The value of impedance when the frequency tends to infinite is the value of RS appreciated in Figure 29a.

The metal/polymer and the polymer/solution capacitances for this model also show an increasing behavior, as the charge density increases. This is explained because more charge is accumulated in a thicker polymer layer.

4.3.2 Macdonald's model fitting

For the implementation of this equivalent circuit, the appropriate predefined circuit is the circuit E. The equivalent circuit structure is presented in Figure 30.

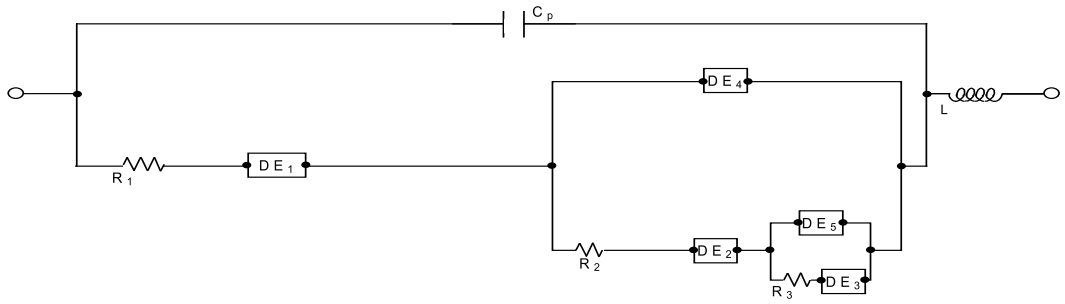

Figure 30: Pre-defined circuit E, included in the LEVMW manual.

Parameter assignment is different, because this circuit includes different components. The complete "P" parameter association is shown in Table 4.2.

Table 4.2: Parameter association for circuit E in the LEVMW software.

Element	Label		Element	Label		Element	Label
RDE1	P(1)		RDE3	P(11)		RDE5	P(21)
TDE1	P(2)		TDE3	P(12)		TDE5	P(22)
UDE1	P(3)		UDE3	P(13)		UDE5	P(23)
PDE1	P(4)		PDE3	P(14)		PDE5	P(24)
NDE1	P(5)		NDE3	P(15)		NDE5	P(25)
RDE2	P(6)		RDE4	P(16)		R1	P(26)
TDE2	P(7)		TDE4	P(17)		R2	P(27)
UDE2	P(8)		UDE4	P(18)		R3	P(28)
PDE2	P(9)		PDE4	P(19)		CP	P(29)
NDE2	P(10)		NDE4	P(20)		L	P(30)

In this circuit, the DE1 block is a distributed element, and it can be replaced with several small equivalent sub-circuits. Each sub-circuit contains a specific model with different physical meaning and mathematical representation. For example, a distributed element can be replaced with a short circuit, with an RC parallel combination, or even with a Warburg element, which is an infinite RC transmission line. The complete table of available sub-circuits can be found in the user's manual of LEVMW software. Some of the most common distributed elements are shown in Table 4.3.

Table 4.3: Available distributed elements and NDE parameter assignment.

NDE	Description
0	Short circuit
1	RC parallel
2	Distributed CPE #1
3	Distributed CPE #2
4	ZC #1 Cole-Cole (Z-level)
5	ZC #2
9	Generalized finite Warburg
15	General diffusion #1
16	General diffusion #2

Selection of the replacement circuit is achieved by assigning the number of the circuit to the NDE parameter. For example, if the NDE1 parameter is set to 1, the distributed element DE1 from Figure 30 is replaced with the circuit shown in Figure 31a. If the NDE1 parameter is set to 2 , the distributed element DE1 is replaced with the circuit displayed in Figure 31b. The RDE, TDE, UDE and PDE parameters change according to the selected equivalent circuit. Specific parameter assignment for each of the individual sub-circuits is detailed in the LEVMW's user manual.

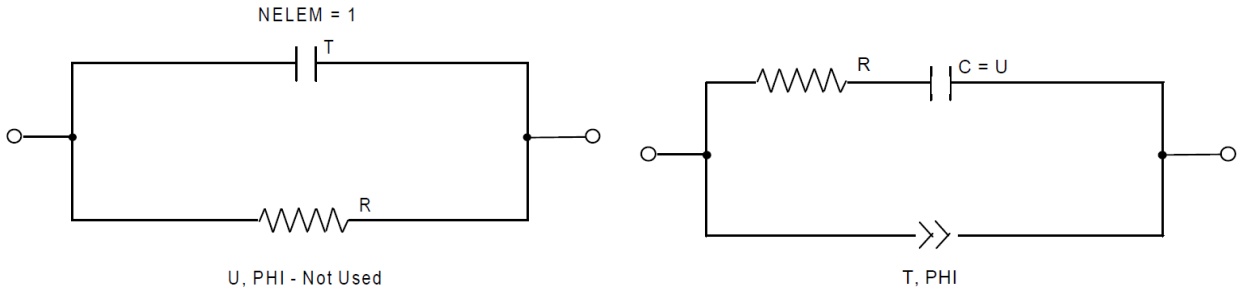

(a) RC Parallel (NDE = 1). (b) Distributed CPE #1 (NDE = 2).

Figure 31: Two distributed elements available in the software.

In order to configure the software to achieve the exact representation of Macdonald's model, there are two distributed elements that need to be replaced: DE4 and DE5. They should be replaced with a pure capacitor. This is achieved by setting parameters P(20) = 1 and P(25) = 1 (an RC parallel) and setting the respective resistances P(16) and P(21) to zero. The capacitance values are accesible at P(17) and P(22), which are set free with a positive value restriction. The rest of the elements needed are P(26), P(27), P(28) and P(29). They also are set free with a positive value restriction. Parameters not used were set to zero, to remove them from the circuit and calculations.

The resulting circuit after these configuration steps is the one observed in Figure 16. The experimental results for electrodes with surface area of 1,0 mm^2 are shown in Figure 32.

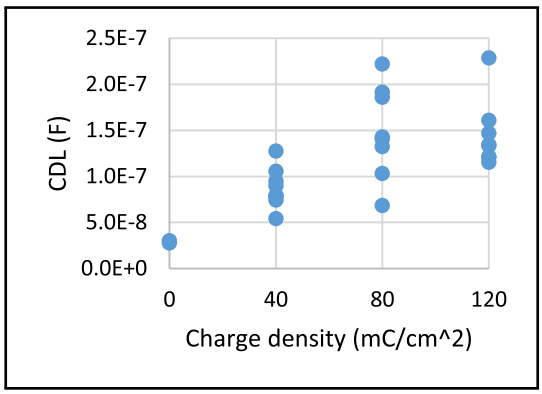

(a) Double-layer capacitance.

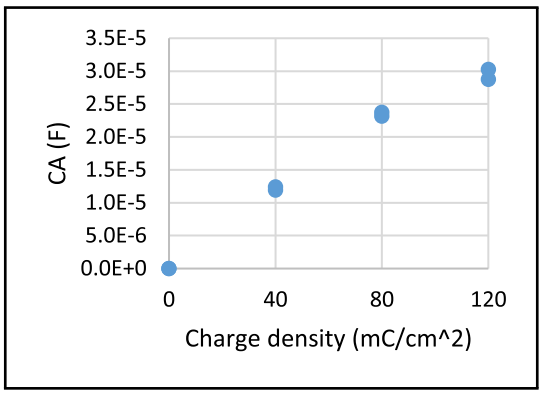

(b) Adsorption capacitance.

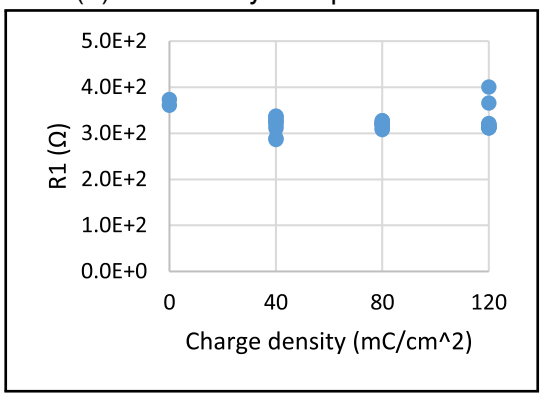

(c) Solution resistance.

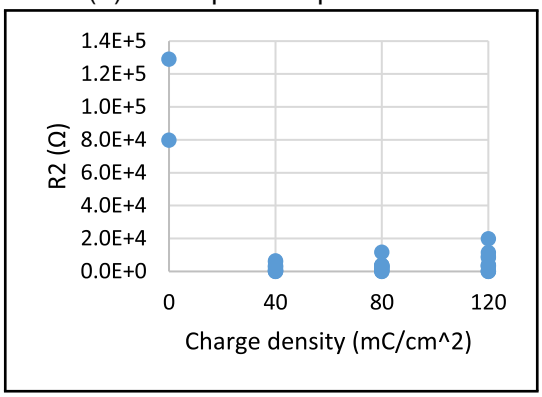

(d) Reaction resistance.

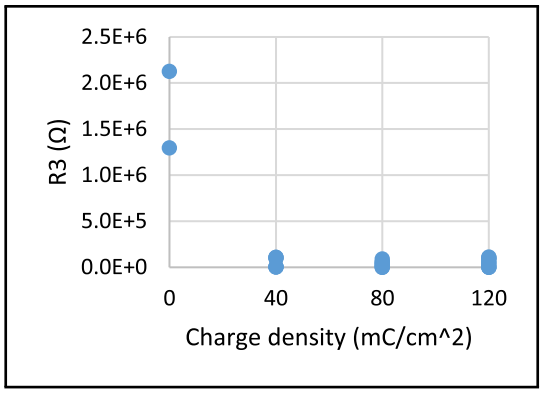

(e) Adsorption resistance.

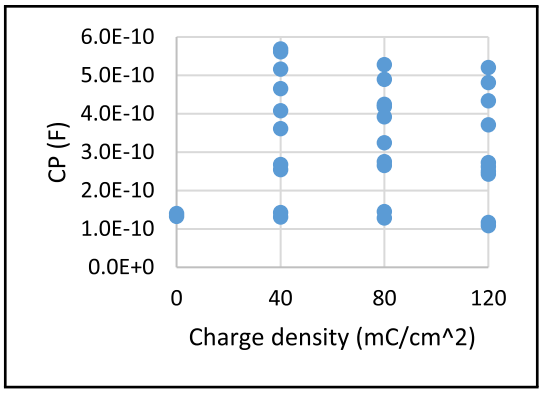

(f) Geometrical capacitance.

Figure 32: Fitting results for the Macdonald's model.

The double-layer capacitance in (a) and the adsorption capacitance in (b) follow both the expected linear trend, which is consistent with the theoretical background and the results from the previous models.

4.3.3 Voigt Model with three RC elements fitting

For the Voigt model with three RC elements, the appropriate model is again circuit A. In order to configure the circuit, parameters P(1), P(2), P(3), P(4) P(5), and P(21) are set free with a positive value restriction, which gives the three RC circuits. The series resistance RS is achieved with the distributed element 1, setting P(6) free for the resistance value.

Here we want to configure the distributed element DE1 as a simple resistance. To achieve this, the NDE parameter P(10) is set to 1. This configures the distributed element DE1 as an RC parallel combination. Then the TDE1, UDE1 and PDE1 parameters P(7), P(8) and P(9) are all set to zero, because in this case TDE stands for the capacitance, and the other parameters are not used by the software. Graphical results for electrodes of 1,0 mm^2 are observed in Figure 33.

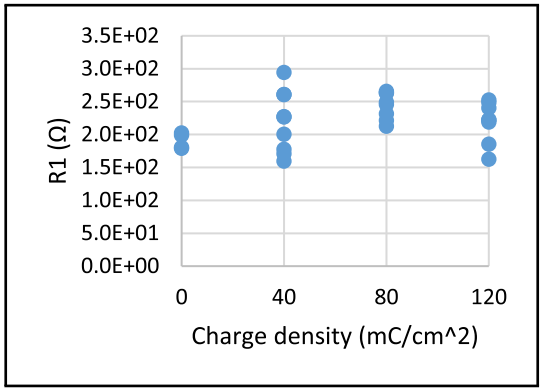

(a) Series resistance.

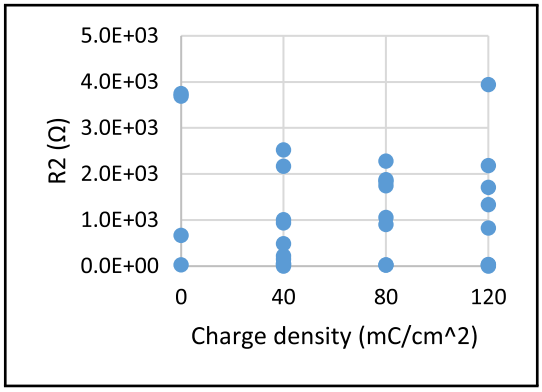

(b) Metal/polymer resistance.

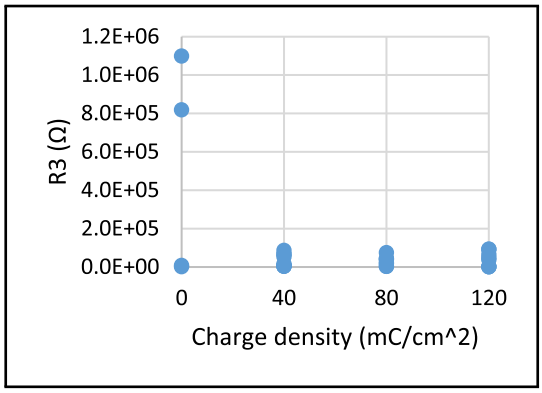

(c) Metal/polymer capacitance.

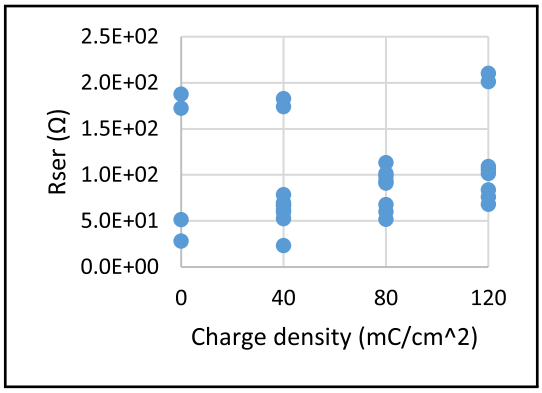

(d) Polymer/solution resistance.

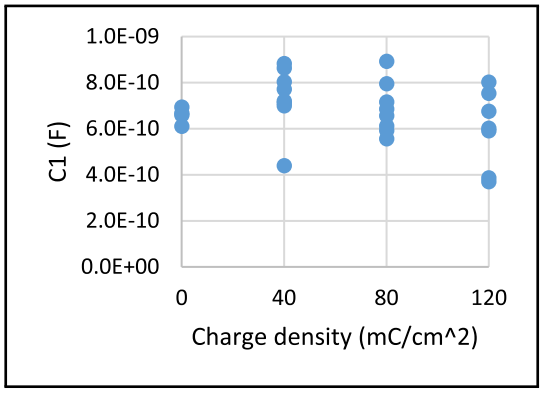

(e) Polymer/solution capacitance.

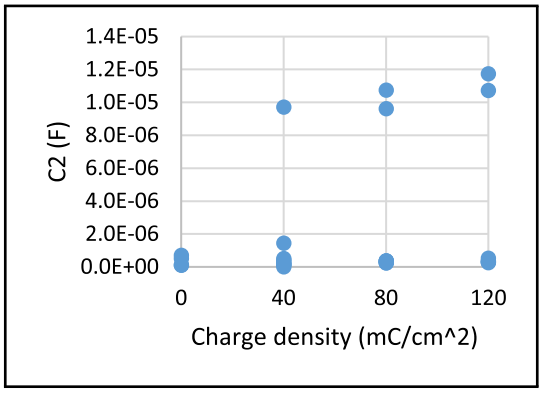

(f) Charge transfer resistance.

Figure 33: Fitting results for the Voigt model (continued in next page).

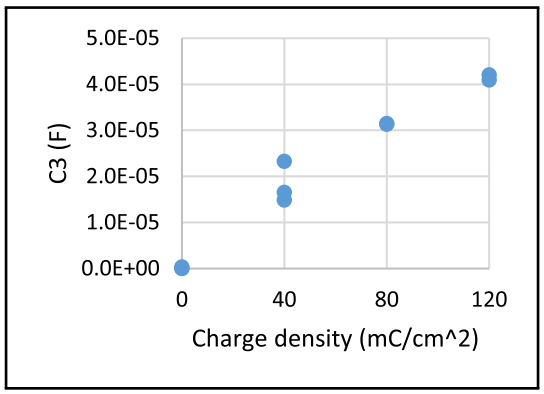

(g) Double-layer capacitance.

Figure 33: Fitting results for the Voigt model (continued).

4.3.4 Bobacka's diffusive model fitting

This model was fitted with MEISP 3.0 because it supports a graphical user interface to perform modifications in the equivalent circuit, and also because it allows parallel processing of multiple datasets. Internally it uses the same Levenberg-Marquardt algorithm present in J.R. Macdonald's LEVMW, so the achieved results are equivalent if the same circuits are used to perform the fittings.

The first step to perform the fitting is to design the equivalent circuit using the graphical user interface. This is shown in Figure 34. With this software, the behavior of the Warburg element can be switched between a shorted-circuit Warburg or an open-circuit Warburg, depending on the experimental conditions. Here we are using the shorted-circuit Warburg because electrode conductivity is high and ions can move freely across the solution.

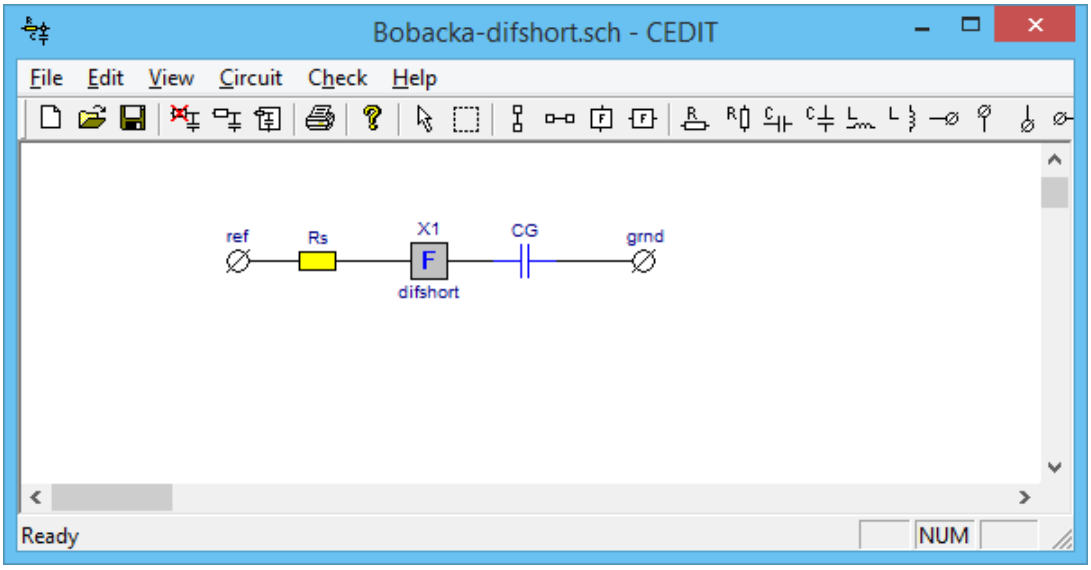

Figure 34: Bobacka diffusion circuit using MEISP 3.0.

After building the model in the schematics editor, a circuit check is required, to make sure that the software understands the design. Internally the software calculates the netlist of the

schematic representation, which is a textual description of the circuit, similar to the Laplace descriptions used to simulate our circuits in MATLAB®. With these expressions, the program can proceed to fit the results to the mathematical expressions by adjusting the constants. The main window of the sofware, with the experimental data loaded and the circuit processed, is shown in Figure 35.

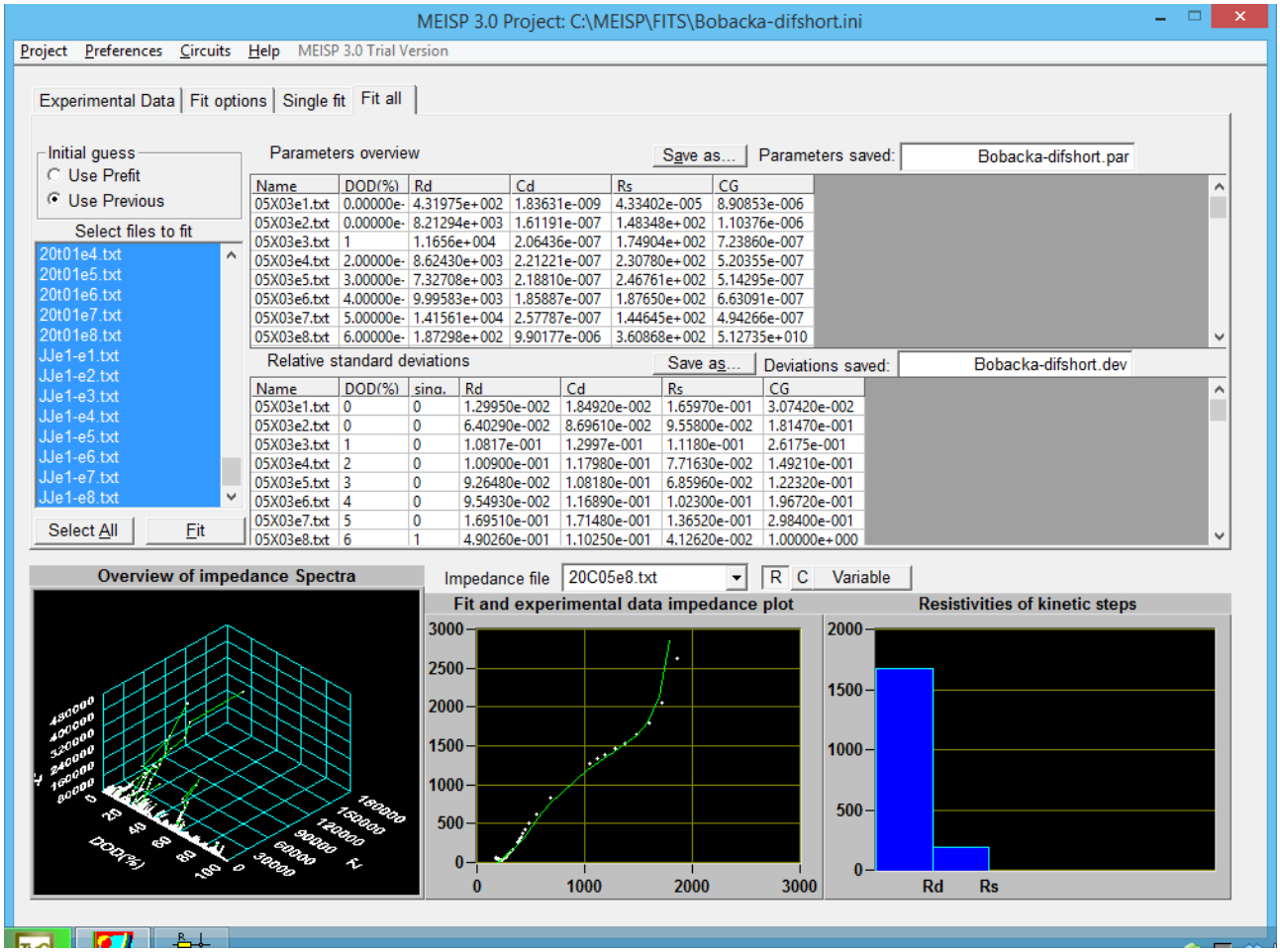

Figure 35: Multiple sample fitting using MEISP 3.0.

Fitting progress is observed in the lower section of the software, and a list of the processed datasets with the achieved parameters is observed in the upper section of this window. This list of parameters is also saved as a text document, separated by tab characters, which is imported then to a Microsoft Excel spreadsheet for further processing in the analysis section of this thesis. This procedure was followed for all models fitted with the MEISP 3.0 software. Actual results of the fitting for this model can be observed in Figure 36.

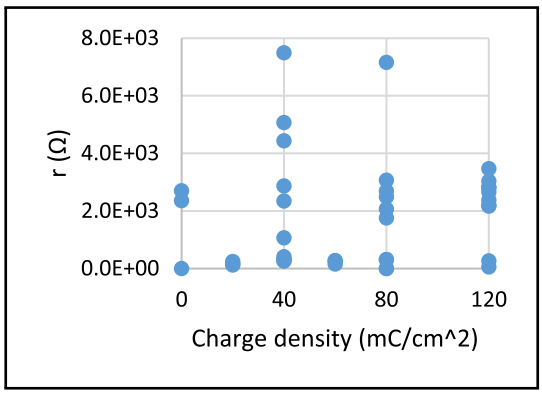

(a) Distributed resistance.

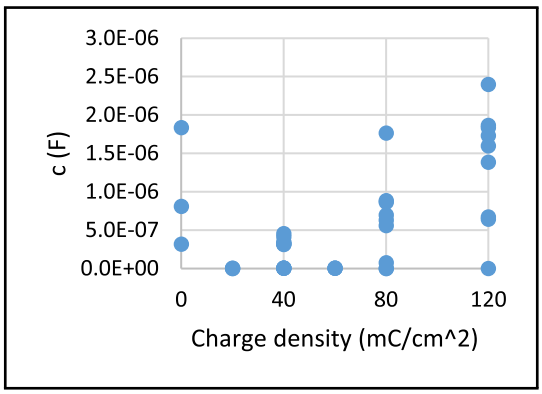

(b) Distributed capacitance.

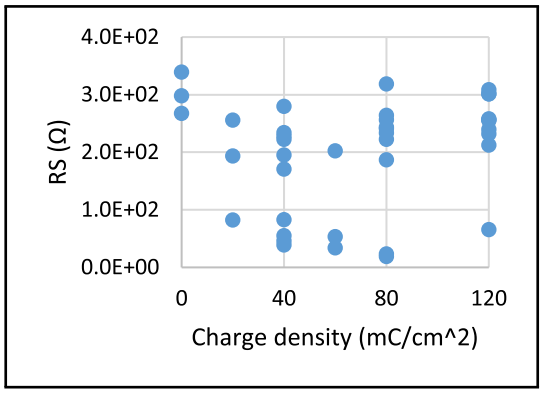

(c) Series resistance.

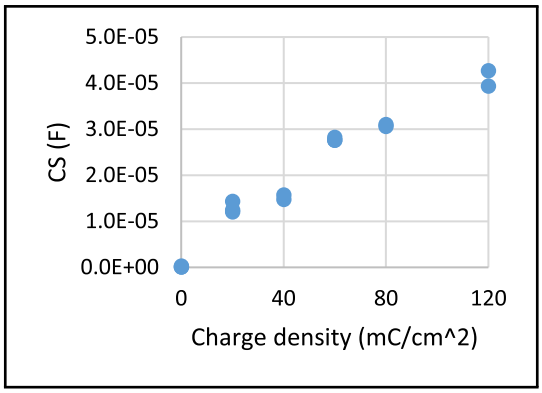

(d) Polymer capacitance.

Figure 36: Fitting results for Bobacka's diffusive model.

As stated in the model review, the capacitance stands for the charge accumulation at the polymer, and it is directly affected by the polymer thickness. The resistance stands for the charge transfer in the electrode, and the Warburg element describes a non-ideal polymer/solution interface, where ions move slower and the signal propagation is not as efficient as in the metal section of the electrode.

4.3.5 Danielsson extension to Bobacka's model

Fitting procedure for this mathematical model is the same as for Bobacka's model: the equivalent circuit is first drawed in the schematics editor, checked for consistency and used in the software to perform the fittings. The results are obtained in a text document, exported to an Excel spreadsheet. Graphical results for electrodes of 1,0 mm^2 can be appreciated in Figure 37.

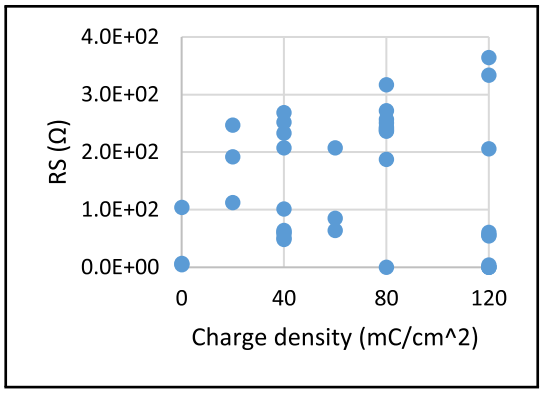

(a) Series resistance.

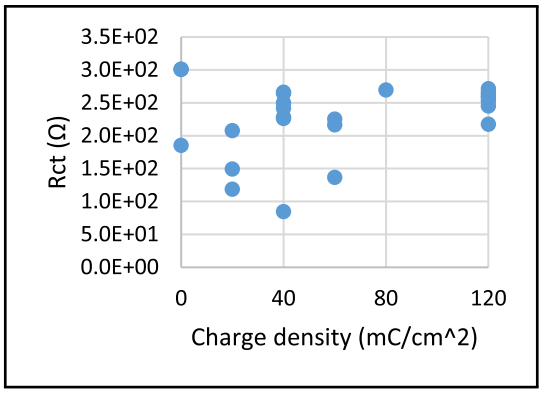

(b) Charge transfer resistance.

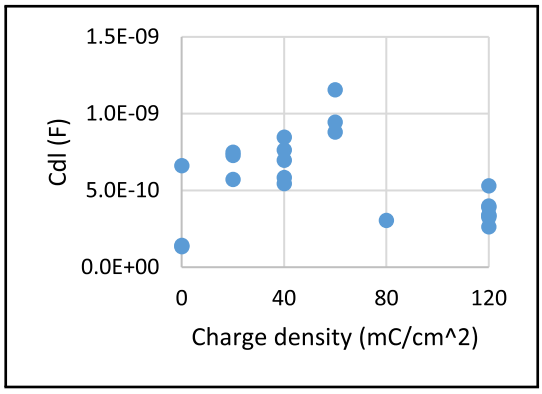

(c) Double-layer capacitance.

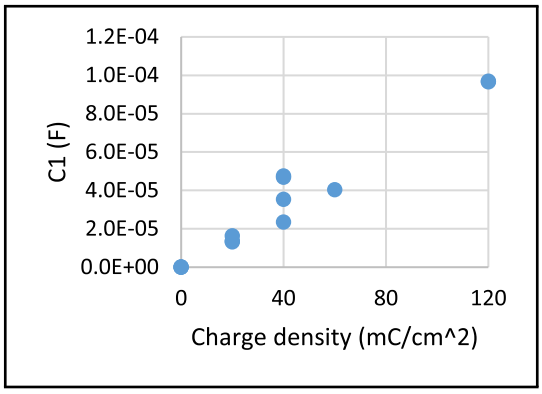

(d) Polymer capacitance.

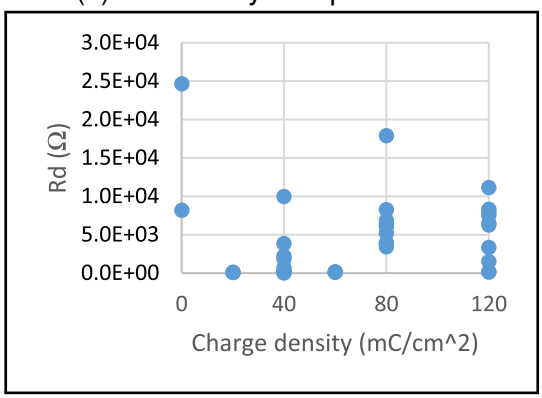

(e) Distributed resistance.

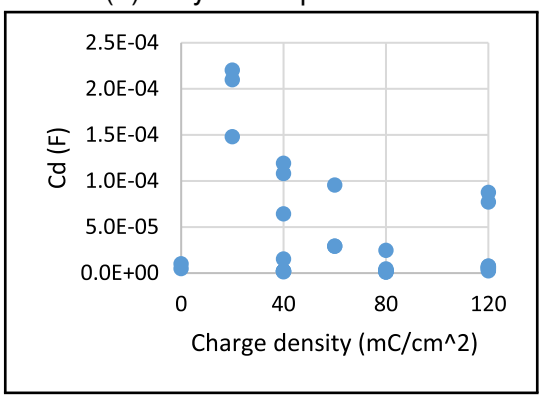

(f) Distributed capacitance.

Figure 37: Fitting results for Danielsson extension of Bobacka's model.

4.4 Comparison between different fittings

It is worth noting that several equivalent circuits were used to fit the same experimental data, and there are some differences between them. In this section, four different equivalent circuits are compared: the double-layer model without geometrical capacitance (which is a Voigt model with two RC circuits in series); the double-layer model with this geometrical capacitance; the model proposed by J.R. Macdonald to describe adsorption of species at an electrode; and the Voigt model with three RC circuits in series.

Graphical results for fitting and simulation of the equivalent circuits are shown in Figure 38. Experimental data is shown in pink circles, and the simulation is shown with a green line. The model of the left is the simple double-layer, the next one is the double-layer with additional geometrical capacitance, and the model of the right is the Voigt model with three capacitors. The order of the system is increased from left to right, as the circuits include more lumped elements.

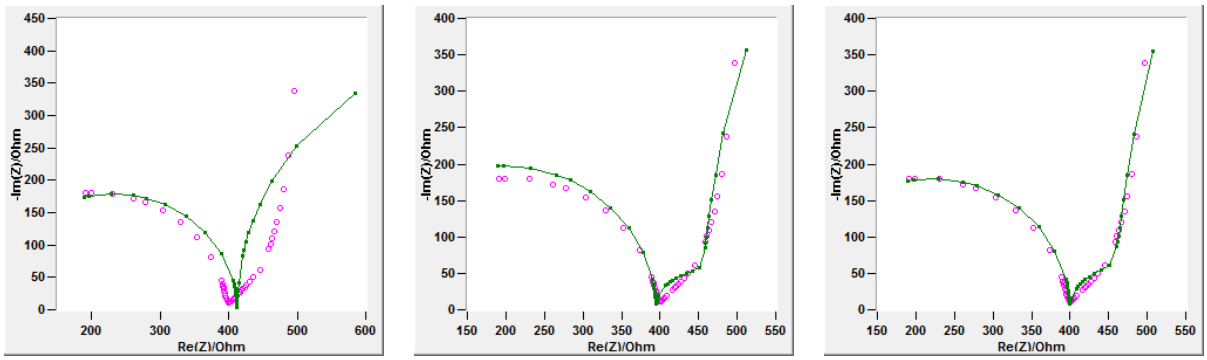

(a) DL model without CG.

(b) DL model with CG, Macdonald's model.

(c) Voigt model with three RC elements.

Figure 38: Fitting comparison between three different models, achieved with MEISP 3.0.

As observed in Figure 38, the fitting results improve as the number of elements of the model increases. The fittings improve also when a distributed element is used, instead of passive ideal elements, because distributed elements provides a better approximation of the physical system, considering that charge is distributed across the ionic solution.

The results suggest that all the six models can be used to describe the electrochemical reactions, but the best fit was obtained with Bobacka's model. This is addressed in the analysis section with the comparison of ANOVA statistics. From the results from Figure 36 and Figure 37, it can be seen that Danielsson's model did not improve the parameter extraction significantly. The best results were obtained with Bobacka's model and can be compared with the experimental results from the author, describing also a metallic electrode coated with a PEDOT layer, in contact with an aqueous solution. The original document from J. Bobacka is found in [16].

All six models show an increase of capacitance when the polymer thickness is increased. This was the expected result. Also, as can be seen from all the experimental graphics, the double-layer capacitance is the one that dominates the behavior of the electrode, because this capacitance is usually between 10 and 100 times higher than other capacitances present in the model. Geometrical capacitance was also about 1000 times smaller than the polymer/solution, and its effects can be neglected.

4.5 Polymerization and model validation

Mathematical models were fitted using experimental data for different charge densities of 0, 40, 80 and 120 mC/cm^2 at the time of deposition. To validate the model, we calculated the expected values for different charge densities, and then measured the values experimentally by a new EIS fitting, to see if the model predictions were according to the experiments. The chosen values of charge density for model validation were 20 mC/cm^2 or 60 mC/cm^2 because they are in the middle of the source data range, and the models have already shown a clear trend in these ranges.

The first step in this section is to prepare the electrodes for the polymerization. The electrode samples are made in a polyimide substrate, where gold is deposited using a mask. A protective coating is deposited in order to expose only the center of the electrodes, which is the active area of the electrode. The electrode structure is shown in Figure 39.

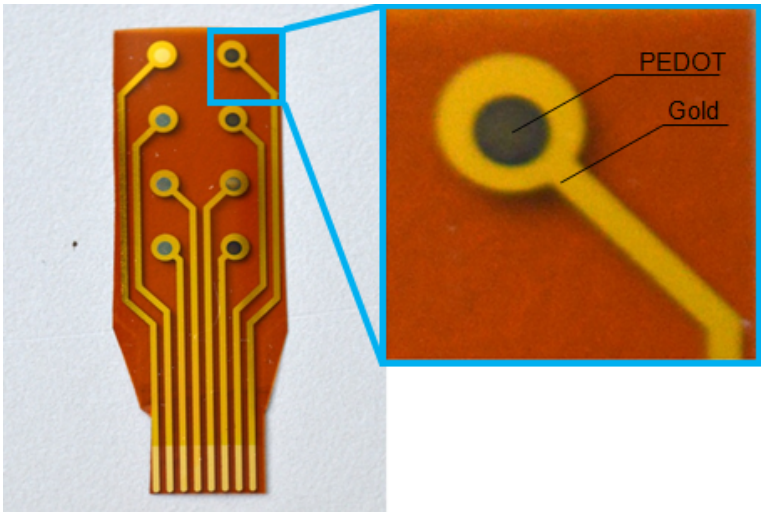

Figure 39: Electrodes with polymer.

Polymerization was done by electrochemical deposition. This technique enables the uniform growth of a thin layer of polymer directly at the exposed surface of the electrodes, by applying an electrical current through the electrode. The experimental procedure is as follows:

1. The working electrode (gold electrode) is dipped in a solution containing the monomer (ethilenedioxythiophene, EDOT) in a known concentration “C”. The electrode has a surface area “A”.

2. The reference electrode is immersed in the same container and is connected to ground.

3. A current of magnitude “I” is applied through the system for a specific time “t”.

Researchers at the TUHH have already found that, in order to achieve a current density of 20 mC/cm^2 with a 1 mm^2 electrode, the applied current required is of 5 µA, and this current should be applied for 40 seconds. To achieve a current density of 60 mC/cm^2 with the same surface area, the current is also 5 µA and deposition time is 120 seconds. The applied current is maintained, and polymerization time determines the final thickness of the polymer.

The laboratory equipment required to perform the polymerization is shown in Figure 40. It is a voltage/current generator that can apply a fixed current for an specific amount of time.

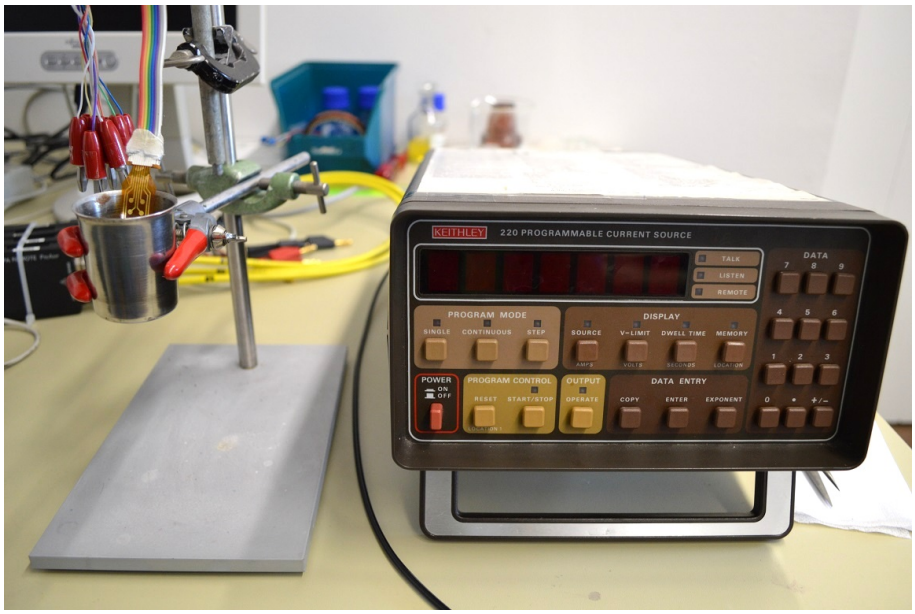

Figure 40: Current generator and polymerization chamber.

After the polymerization is completed, the electrode and the polymerization chamber are cleaned with deionized water. Then, the chamber is filled with a commercial irrigation solution, the electrode is dipped in it, and the EIS experiments are performed with an Agilent 4284A LCR meter, which applies a fixed AC voltage to the electrode and sweeps the frequency from 20 Hz to 1 MHz. The LCR meter is shown in Figure 41.

Figure 41: Agilent 4284A LCR meter for performing the EIS characterization.

The electrodes are analyzed one by one, leaving the other seven electrodes disconnected, removing them from the system. The experimental results for this newly fabricated electrode can be appreciated in Figure 42.

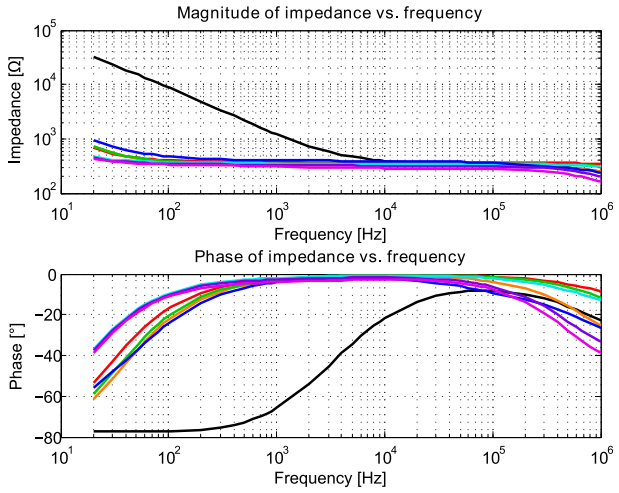

(a) Bode plots of the experimental data.

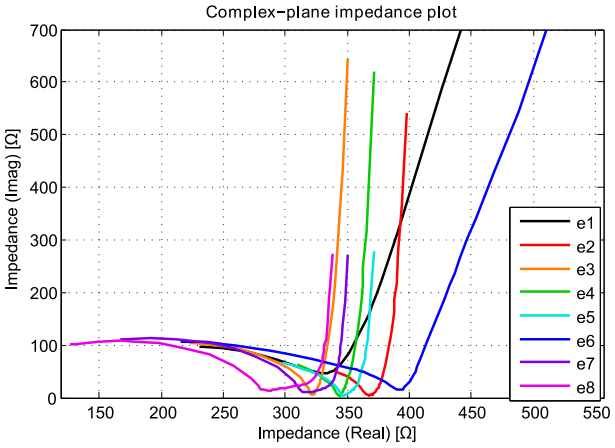

(b) Nyquist plots of the experimental data.

Figure 42: Bode and Nyquist plots of experimental data for test sample “Au10JJe1”.

The next step is to perform the fittings for the experimental results. These fittings are done using the same equivalent circuits detailed in the last section of this document. The achieved fittings were consistent with the results obtained previously.

Bobacka’s model shows a clear trend in the bulk capacitance of the polymer film, as can be observed in Figure 43. Points in **blue** are taken from the experimental fittings of the original data set. These results exhibit a linear trend, with a correlation coefficient R^2 = 0,9888. The equation for the original trend is $CS = 3,46058 \times 10^{-7} \cdot CD + 9,73143 \times 10^{-7}$ and this trend is displayed in blue. The 1-way ANOVA for this data trend gives a P-value of 0.0000182451 which shows statistical significance.

Points displayed in **red** are the fitted results of the experiments performed in this section. As can be appreciated in Figure 43, these results are not far away from the original model, and can be included in the linear regression calculation to obtain the final trend of capacitance.

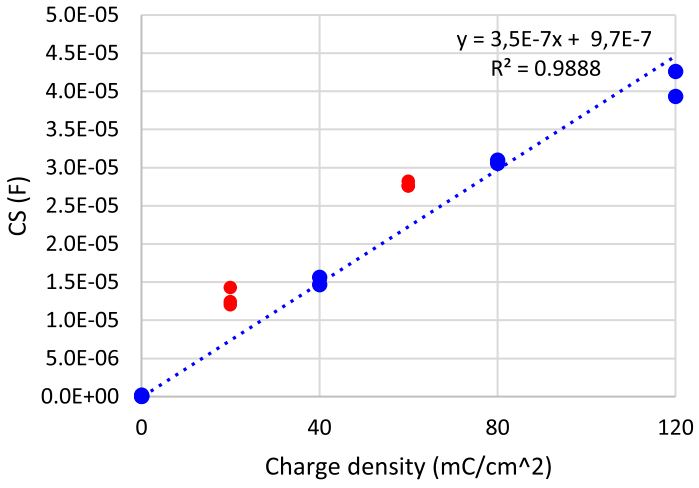

Figure 43: Bulk capacitance of the polymer film as a function of the charge density.

An updated linear regression was performed to include the results from all the experiments, including the newly fabricated samples. The final plot of electrode effective capacitance versus charge density can be appreciated in Figure 44. The results show statistical significance when applying a 1-way ANOVA for the total population (F = 522.5630571, P = 8.3828E-11).

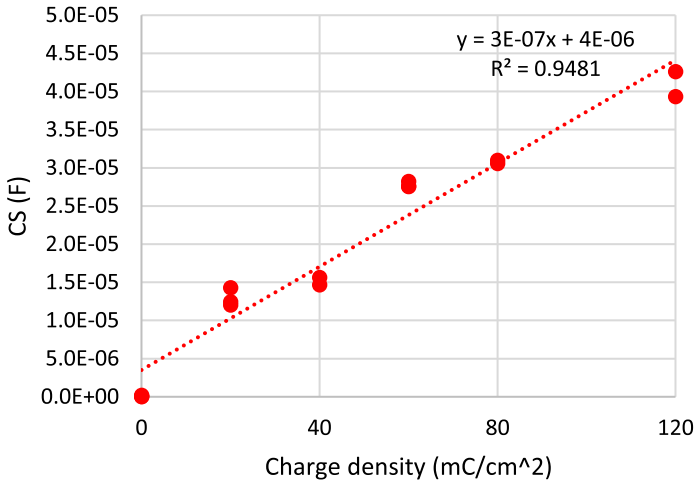

Figure 44: Bulk capacitance of the polymer film as a function of the charge density.

Chapter 5

Analysis

In this chapter we apply statistical methods to analyze the fitting results. These methods include outlier detection using Dixon's q-test, one-way analysis of variance (ANOVA) and linear regression methods to extract useful information from our large set of data.

The first section of this chapter is an explanation of the statistical methods used. These are the Dixon's q-test for outlier detection, and the one-way analysis of variance (1-way ANOVA). Also, linear regression was used to extrapolate some of the extracted parameters.

The second part contains some examples of the application of statistical methods to our data. We analyzed all our data using these methods, but it is impractical to place here all the results for our complete set of 96 electrodes. We apply here the ANOVA method to study populations where the electrode area is of 1,0 mm^2, for only the double-layer model. This was repeated for the complete set of models in order to measure the statistical significance of the fitting results.

And the third section of this chapter shows the final results for important physical variables, such as the solution resistance, and the total double-layer capacitance (PEDOT/solution interface) of the electrodes.

5.1 Statistical methods

5.1.1 Dixon's q-test for outlier detection

Dixon's q-test is a valid method for outlier identification and data discarding from a statistical population. This method compares the value of the extreme values with their nearest neighbors, to establish a quotient that can be used for discarding the suspected value. The calculated quotient Q_{exp} is compared with tabulated values of Q_{crit} considering different confidence levels. A complete study of critical values for samples up to 100 elements is found in [19], with the proper tables for comparison and data discarding.

The equation used to calculate the experimental quotient, Q_{exp}, is:

$$Q_{exp} = \frac{s_x - s_{x-1}}{s_{max} - s_{min}}$$

Where

- s_x is the suspected value,
- s_{x-1} is its nearest neighbor,
- s_{max} is the maximum value in the population,
- s_{min} is the minimum value in the population.

If $Q_{exp} > Q_{crit}$ then the suspected value can be considered an outlier, within the apropriate confidence level obtained from the table, and can be safely removed from the population. This was oner of the methods used to discard experimental values that were suspected as outliers.

5.1.2 Additional data discarding considerations

Another method used to discard experimental data was by a general inspection of the results: usually the output values for any parameters are suspected to be within a specific range. If the value is relatively high (with exponents greater than 1E+10) then they are discarded because the fitting does not have any physical significance: the parameter is considered as divergent, because it is introducing noise to the rest of the fittings, and it is safely removed too.

The last method used to discard data was selecting parameters relatively closed to zero (when comparing to the rest of the data within the electrode sample), because this could indicate that the parameter was not needed in the fitting process and the algorithm could have achieved convergency even if the parameter were fixed to zero. This discards the lowest part of the capacitance graphics, enabling to leave only the data points that exhibit a clear trend of statistically significance, and these trends are comparable with other experiments achieved by different research teams. The complete list of fitted results without modification is available in a Excel spreadsheet, and the final results after discarding all the suspected values are also available in another spreadsheet, with the statistical calculations for finding trends and proving statistical significance.

5.1.3 Analysis of variance (ANOVA)

The Analysis of Variance (ANOVA) is a statistical tool useful to compare the mean values of datasets, grouped by one or more treatment. A “treatment” is defined as one input variable that is suspected to influence the behavior of the output variable. There are different types of ANOVA, and in this Master’s thesis we used the one-way ANOVA.

One-way ANOVA is a method that can be used to prove if the mean values of different measurements are similar (which means that the experimental data is not of statistical significance, because the effect of the “treatment” is irrelevant on the output variable), or if they are clearly differentiated and can used to calculate a trend.

The F value is obtained from the F-test and it is a ratio of the variance between the sample and between groups. The p-value is used to reject the null hypothesis, where all the mean values are equal. If the p-value is less than a critical value, typically 0,05 then the null hypothesis can be rejected, and the mean values are different enough to suspect that the “treatment” affects the dependent variable.

We have used this statistical tool to measure the significance of our fitting results, specifically for the polymer/solution capacitance, that was found to be linearly dependent on the charge density. In the following sections we provide some examples of how to perform an ANOVA calculation, some example tables and the results for the data among the six studied models.

5.2 Data analysis examples

5.2.1 Solution resistance vs. charge density

In this analysis, the treatment is the charge density (CD) and it is suspected that this variable could affect the solution resistance (RS), which is the output variable. Data has been obtained by fitting the experimental results for an electrode of 0.5 mm^2 using the double-layer model. The first step is to separate the fitting results in four columns, one for each independent measurement condition. The input data of the ANOVA test is shown in Table 5.1.

Table 5.1: Calculated values of the solution resistance RS (Ω), for different charge densities CD using the double-layer model with an electrode size of 0.5 mm^2.

N	**0**	**40**	**80**	**120**
1	488.08375	417.49958	428.97650	395.76348
2	471.65553	403.66614	411.54236	394.86809
3		414.13140	408.50303	405.10882
4		410.97605	437.67799	708.96854
5		408.18159	416.13772	427.67111
6		420.90255	411.85025	390.30087
7		429.69525	410.98130	414.18598
8		442.04111	454.94904	405.70491
9		408.60604	424.13683	421.81614
10		410.56155	400.40585	397.20735

Before doing the ANOVA test, I suspected that the resistance value of 708.96854 was too high when compared with the rest of measurements. To be able to remove this value from the statistics, I applied the Dixon's Q-test, which is used for identification and exclusion of outliers. The calculation is shown in the next equation, where x_s is the suspected value, x_{s-1} is the nearest value from the suspected value, x_n is the maximum value of all the data set, and x_1 is the minimum value.

$$Q_{exp} = \frac{x_s - x_{s-1}}{x_n - x_1} = \frac{708.96854 - 488.08375}{708.96854 - 394.86809} = \frac{220.88479}{314.10045} = 0.7032$$

We have 32 observations, so we must look for a Q_{crit} value in a proper table. If $Q_{exp} > Q_{crit}$ then the value can be rejected. But if $Q_{exp} > Q_{crit}$ then the suspected value must be preserved and used in the statistical calculations. A complete table of Q_{crit} values can be found in [19]. For a set of 32 samples, the critical value for a confidence level of 99.5% is 0.3646 so in this case $Q_{exp} > Q_{crit}$ and the suspected value can be discarded. The value 708.96854 will not be used in the rest of the statistic calculations.

The results of the ANOVA test for data of Table 5.1 are presented here:

Table 5.2: ANOVA results for solution resistance vs. charge density in electrodes of 0.5 mm^2 using the double-layer model.

Param	VALUE	Param	FACTOR	ERROR
F	16.0621	df	3	27
Pval	0.000003	SS	9045.6	5068.47
Sxp	13.7011	MS	3015.2	187.721

The results of this ANOVA suggests that the solution resistance is dependent on the charge density applied at time of the deposition, because the P value is smaller than the critical value of 0,05. This means that the mean values of the data present in Figure 45 are different between them, and it is correct to look for a trend using regression techniques.

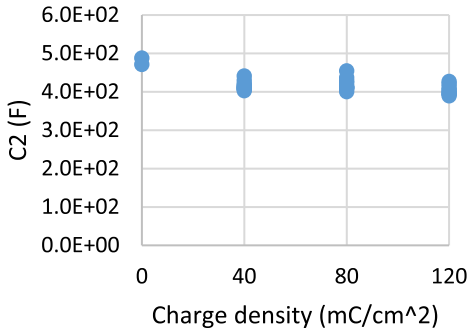

Figure 45: Solution resistance as a function of the charge density (double-layer model).

5.2.2 Solution resistance vs. electrode size

In this case, the treatment is the electrode size. We suspect that the electrode size influences the effective value of the solution resistance, which was the expected result by observing the Bode plots of Figure 24. To perform the ANOVA calculation, we need to sort the data in three columns, as shown in Table 5.3.

Table 5.3: Calculated values of the solution resistance RS (Ω), for different electrode sizes, using the double-layer model.

N	**0.5**	**1.0**	**2.0**
1	488.08375	373.29851	261.11843
2	471.65553	360.95162	255.90769
3	417.49958	289.37962	224.40022
4	403.66614	338.04797	245.01993
5	414.13140	323.25548	246.54926
6	410.97605	336.45855	233.27830
7	408.18159	332.46323	240.14346
8	420.90255	327.01401	243.11209
9	429.69525	337.27717	243.65036
10	442.04111	286.57310	244.56144
11	408.60604	311.16777	199.38436
12	410.56155	317.30824	248.32339
13	428.97650	317.35637	226.64582
14	411.54236	323.47757	219.92714
15	408.50303	327.42259	232.44349
16	437.67799	318.76402	228.99956
17	416.13772	310.18365	234.38493
18	411.85025	303.13969	247.16791
19	410.98130	318.96095	192.76770
20	454.94904	326.89240	215.73435
21	424.13683	308.24216	209.32584
22	400.40585	320.50681	210.70123
23	395.76348	311.47270	223.16982
24	394.86809	400.39414	244.25963
25	405.10882	365.93786	249.67990
26	708.96854	316.00517	242.34338
27	427.67111	313.56387	255.10582
28	390.30087	312.22989	236.83191
29	414.18598	319.88517	222.83439
30	405.70491	317.55224	228.26819
31	421.81614	320.95642	228.61342
32	397.20735	312.38949	223.64730

The results of the 1-way ANOVA are observed in Table 5.4.

Table 5.4: ANOVA results for solution resistance vs. electrode size, using the double-layer model.

Param	VALUE	Param	FACTOR	ERROR
F	658.675	df	2	92
Pval	3.01555e-55	SS	548862	38331
Sxp	20.4118	MS	274431	416.641

By observing the results of the ANOVA analysis, we can assume that the mean values are different for the three electrode sizes, because the P value is much less than 0,05 for this dataset. This means that the solution resistance shows a strong influence on the size of the electrode. The graphical results for this behavior is shown in Figure 46.

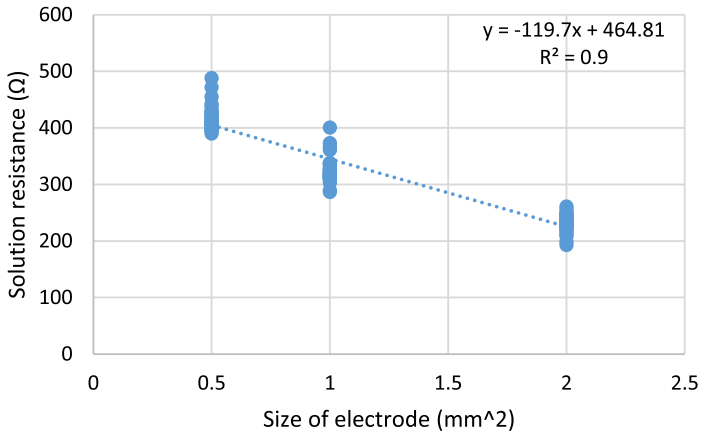

Figure 46: Solution resistance as a function of electrode size.

5.2.3 Capacitance of the PEDOT/solution interface

One of the significant results of this master's thesis is the study of the behavior of the polymer/solution capacitance as a function of the charge density. This capacitance was found to be around 10 and 100 times higher than the capacitance in the gold/polymer interface, as can be seen when comparing the plots in Figure 47 with the fitting results performed in the previous chapter.

As can be appreciated in Figure 47, the six mathematical models studied in this master's thesis show a clear trend in the polymer/solution capacitance, depending on the charge density. This means that if the polymeric coating is thicker, more charge is accumulated in the polymer/solution interface.

The fitting results, trends, and linear regression performed for the PEDOT/solution interface capacitances for the six mathematical models can be observed in Figure 47. These models exhibit a linear trend, with a correlation coefficient higher than 90% except for the double-layer model with geometrical capacitance, which exhibit lower correlation.

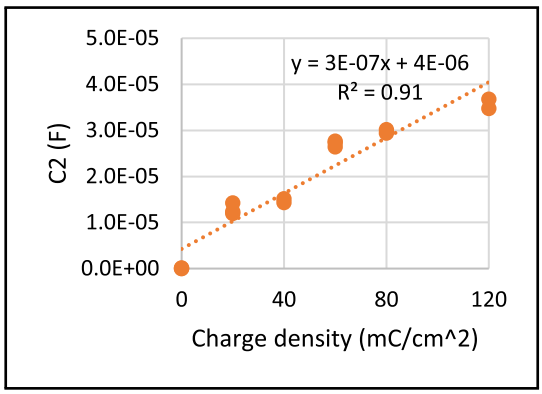

(a) Double-layer model.

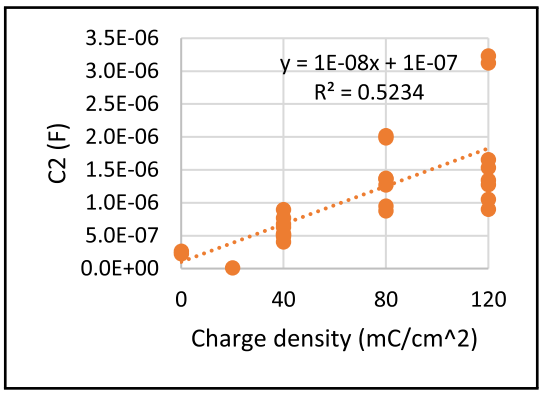

(b) Double-layer with CG.

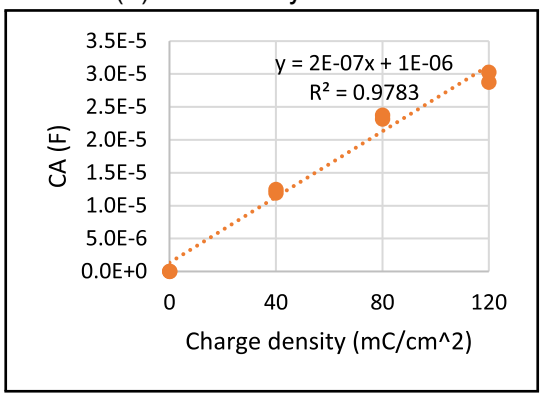

(c) Macdonald's model.

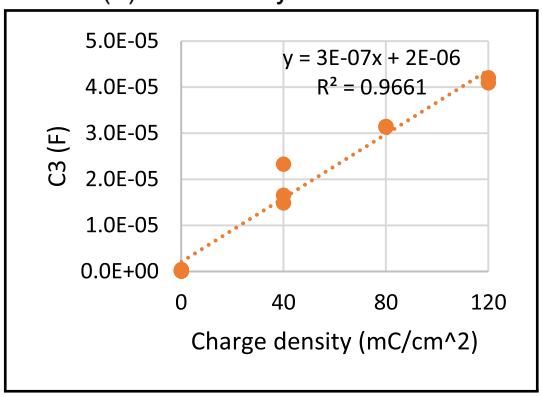

(d) Voigt 3 model.

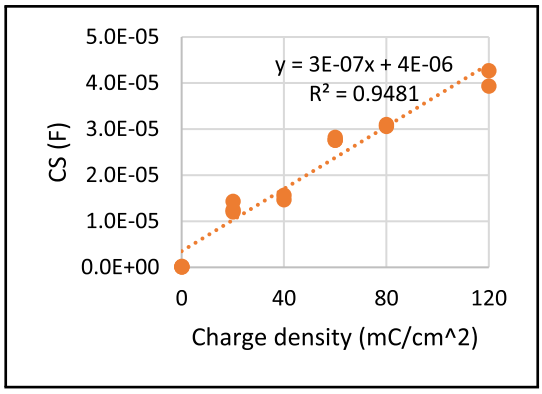

(e) Bobacka's model.

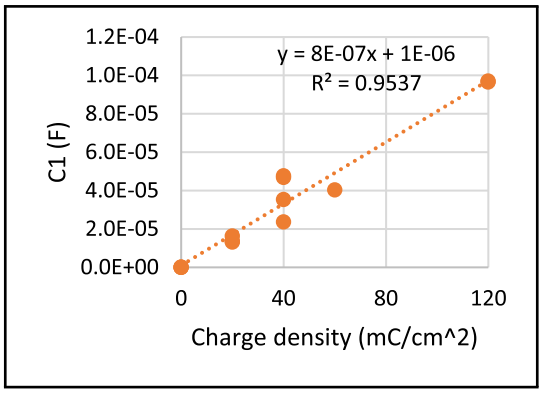

(f) Danielsson's model.

Figure 47: Capacitance of the PEDOT/solution interface for different models.

To be able to compare the quality of the fittings and the relevance of the trends found in these graphics, a one-way ANOVA was calculated for each one of the six models. The results of the ANOVA analysis can be observed in Table 5.5.

Table 5.5: 1-way ANOVA comparison of models (polymer/solution capacitance).

Model	**F**	**P**
DL	6,750722665	0,002126195
DLCG	6,394004139	0,001577311
Macdonald	963,9628455	3,57567E-06
Voigt 3	2,094419305	0,141243076
Bobacka	522,5630571	8,3828E-11
Danielsson	64,42094641	4,01125E-06

As shown in the previous table, the best fitting and clear trend was found with Bobacka's diffusive model, because it features the smallest P value among the studied models. All the mathematical models achieved statistical significance, with P values of less than 0,05. This means that the charge density is one strong factor influencing the double-layer capacitive effect.

The main conclusion of this analysis is that the electrode behavior is dominated by the polymer/electrolyte capacitance, and this indicates that a thicker polymer coating results in a higher capacitance at this interface. This was found in the six mathematical models studied, and it is in accordance with the theory and with other experimental results from different research groups. For example, J. Bobacka [16] obtained the same bulk capacitance trends, depending on the charge density at time of deposition.

Chapter 6

Conclusions

- The polymer/solution capacitance was found to be around 10 – 100 times higher than the metal/polymer capacitance and therefore is the predominant capacitance in this system.
- EIS fitting was performed for six mathematical models, and the fitting results were statistically significant for studying the capacitance in the electrode/solution interface, as confirmed by the 1-way ANOVA ($p < 0,05$).
- Diffusive models achieved better fits than ideal-element models, as can be appreciated by the 1-way ANOVA analysis. The best fit was achieved with Bobacka's diffusive model, with the lowest P value for ANOVA statistics ($F = 522.5630571$, $p = 8.3828E-11$).
- Models were validated by fabricating new electrodes and comparing extrapolated values with fitted values, obtaining a correlation coefficient (R^2) of 94,81% for the complete set of data.
- Electrode performance is dominated by the polymer/solution capacitance, which increases linearly with the thickness of the polymer, with a correlation coefficient (R^2) greater than 90% for all the cases except the Double-layer model with CG, where R^2 is of 52,34%. The linear trend found in the polymer/solution is explained because charge is accumulated in a thicker polymeric layer. This result is in accordance with the experimental results of other research groups.

TUHH
Technische Universität Hamburg-Harburg

Institut für Nanoelektronik
Nanoelectronics
Prof. Dr. Wolfgang Krautschneider

Hamburg University of Technology – E-9 – D-21071 Hamburg

Mailing address:
D-21071 Hamburg, Germany

Visitors:
Eissendorfer Str. 38
D-21073 Hamburg, Germany

Phone: +49-40-42878-3030
Fax: +49-40-42878-2877
e-Mail: krautschneider@tu-harburg.de

14. März 2013

Letter of Invitation for Mr. Juan José Montero-Rodríguez

Herewith I invite Mr. Juan José Montero-Rodríguez for a stay at the Institute of Nanoelectronics at the Technische Universität Hamburg-Harburg in order to carry out his Master´s thesis for the Master´s Program in Microelectromechanical Systems of the Instituto Tecnológico de Costa Rica.

For his master´s thesis topic, Mr. Montero-Rodríguez will focus on the improvement of the electrode/tissue interface using conductive polymer coating in medical applications, as part of the joint efforts of the Institute of Nanoelectronics and the Institute of Electronic and Optical Materials, where our research aims to use novel polymeric coatings and nanostructured materials in order to achieve better electric behavior and mechanical performance of the electrode/tissue interface in medical electrodes. The study is now focused on two different nanostructures applied onto the electrode surfaces: vertically aligned nanotubes and nano-porous polymeric aerogels.

During his stay, I will supervise Mr. Montero-Rodríguez as Director of the Institute of Nanoelectronics. After a careful review of the research proposal, I determined that all proposed activities can be carried out within 6 months. Mr. Montero-Rodríguez will be permitted to use the full infrastructure of the Institute of Nanoelectronics. This includes the computer pool, software pool and the laboratories.

Kind regards,

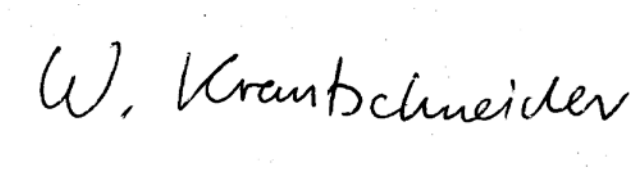

Prof. Dr.-Ing. habil. W. Krautschneider
Director
Institute of Nanoelectronics

Bibliography

[1] C.K. Chiang, C.R. Fincher, Y.W. Park, A.J. Heeger, H. Shirakawa, E.J. Louis, S.C. Gau, and A.G. MacDiarmid. Electrical conductivity in doped polyacetylene. *Physical Review Letters*, 39(17):1098–1101, 1977.

[2] M Asplund, E Thaning, J Lundberg, a C Sandberg-Nordqvist, B Kostyszyn, O Inganäs, and H von Holst. Toxicity evaluation of PEDOT/biomolecular composites intended for neural communication electrodes. *Biomedical materials (Bristol, England)*, 4(4):045009, August 2009.

[3] AJ Heeger. Nobel Lecture: Semiconducting and metallic polymers: The fourth generation of polymeric materials. *Reviews of Modern Physics*, 73(July):681–700, 2001.

[4] Rajeswari Ravichandran, Subramanian Sundarrajan, Jayarama Reddy Venugopal, Shayanti Mukherjee, and Seeram Ramakrishna. Applications of conducting polymers and their issues in biomedical engineering. *Journal of the Royal Society, Interface / the Royal Society*, 7 Suppl 5:S559–79, October 2010.

[5] Ricardo Starbird, Wolfgang Krautschneider, Grit Blume, and Wolfgang Bauhofer. In Vitro Biocompatibility Study and Electrical Properties of the PEDOT, PEDOT Collagen-Coat, PEDOT Nanotubes and PEDOT Aerogels for Neural Electrodes. In *Biomedical Engineering (BioMed 2013)*, pages 320–326, Innsbruck, Austria, 2013.

[6] Karen C. Cheung and Philippe Renaud. BioMEMS for medicine: On-chip cell characterization and implantable microelectrodes. *Solid-State Electronics*, 50(4):551–557, April 2006.

[7] Karen C Cheung, Philippe Renaud, Heikki Tanila, and Kaj Djupsund. Flexible polyimide microelectrode array for in vivo recordings and current source density analysis. *Biosensors & bioelectronics*, 22(8):1783–90, March 2007.

[8] Andrzej Lasia. Electrochemical impedance spectroscopy and its applications. *Modern aspects of electrochemistry*, 32:143–248, 2002.

[9] J. Ross Macdonald and Evgenij Barsoukov. *Impedance Spectroscopy: Theory, Experiment and Applications*. Wiley, 2005.

[10] XZ Yuan, C Song, H Wang, and J Zhang. EIS Equivalent Circuits. In *Electrochemical Impedance Spectroscopy in PEM Fuel Cells*, pages 139–192. Springer, 2010.

[11] ME Orazem, P Agarwal, and LH Garcia-Rubio. Critical issues associated with interpretation of impedance spectra. *Journal of Electroanalytical Chemistry*, 378:51–62, 1994.

[12] J.Ross Macdonald. Impedance/admittance response of a binary electrolyte. *Electrochimica Acta*, 37(6):1007–1014, May 1992.

[13] JE Bauerle. Study of solid electrolyte polarization by a complex admittance method. *Journal of Physics and Chemistry of Solids*, 30:2657–2670, 1969.

[14] Evgenij Barsoukov. Evgenij Barsoukov's collection of impedance spectroscopy resources. http://impedance0.tripod.com/. Accessed November 29, 2013.

[15] J.-B. Perez-Navarrete. Establishment of Electrical Equivalent Circuits from electrochemical impedance spectroscopy study of corrosion inhibition of steel by imidazolium derived ionic liquids in sulphuric acidic solution. In *2010 7th International Conference on Electrical Engineering Computing Science and Automatic Control*, pages 225–229. IEEE, September 2010.

[16] Johan Bobacka, Andrzej Lewenstam, and Ari Ivaska. Electrochemical impedance spectroscopy of oxidized poly (3, 4-ethylenedioxythiophene) film electrodes in aqueous solutions. *Journal of Electroanalytical Chemistry*, 489:17–27, 2000.

[17] Petter Danielsson, Johan Bobacka, and Ari Ivaska. Electrochemical synthesis and characterization of poly(3,4-ethylenedioxythiophene) in ionic liquids with bulky organic anions. *Journal of Solid State Electrochemistry*, 8(10):809–817, August 2004.

[18] J.E.B. Randles. Kinetics of rapid electrode reactions. *Discussions of the faraday society*, 1947.

[19] SP Verma and A Quiroz-Ruiz. Critical values for six Dixon tests for outliers in normal samples up to sizes 100, and applications in science and engineering. *Revista Mexicana de Ciencias Geológicas*, pages 133–161, 2006.

Equivalent circuit models for electrochemical impedance spectroscopy of PEDOT-coated electrodes

Juan J. Montero-Rodríguez*, Dietmar Schroeder and Wolfgang Krautschneider
Institut für Nano –und Medizinelektronik
Technische Universität Hamburg-Harburg
Hamburg, Germany
Corresponding author e-mail: juan.montero@tuhh.de

Ricardo Starbird
Institut für Optische und Elektronische Materialen
Technische Universität Hamburg-Harburg
Hamburg, Germany

***Abstract*—In this study we implemented six mathematical models to describe the electric performance of 96 neural electrodes coated with a single film of conductive polymer. The experiments were performed in-vitro, reproducing the environment of the implanted electrodes, and impedance was measured using the electrochemical impedance spectroscopy (EIS) method. We found that the double-layer capacitance at the polymer/solution interface is the most representative parameter affecting charge transfer, and observed that this capacitance increases linearly with the polymer thickness.**

I. Introduction

Neural microelectrodes are used to measure electrical signals directly from the brain, and also to stimulate specific areas of it by injecting electrical currents into the tissues. The electrode performance depends on the surface area and also on the materials used in the interfaces.

Electrode performance can be significantly improved by coating the active area of the electrodes with a conductive polymer [1]. This material actively transfers electrons from the metal into ions to the tissue, based on a reduction-oxidation reaction at the electrode surface [2].

Test neural electrodes are fabricated using polyimide as substrate since they are easier to fabricate, manipulate and relative cheaper that commercial electrodes. The impedance of these test electrodes was determined by electrochemical impedance spectroscopy (EIS). This technique gives the impedance of the samples as a function of the frequency.

When the impedance spectrum of the electrodes is known, an equivalent circuit of the experiment can be proposed by inspecting the interfaces between different materials. The experimental data of impedance is fitted to the circuit model to characterize the electrical phenomena at each interface.

In this study, experimental results from 96 electrodes are fitted to six equivalent models found in the literature, in order to determine the influence of fabrication parameters in the electrode performance.

Eight additional electrodes were fabricated with different deposition conditions, to increase the amount of data points required for the linear trends developed in the results.

II. Materials and Methods

Larger versions of neural gold electrodes were fabricated on a polyimide substrate, and coated with a uniform layer of poly(3,4-ethylenedioxythiophene) (PEDOT). The electrodes are shown in Fig. 1.

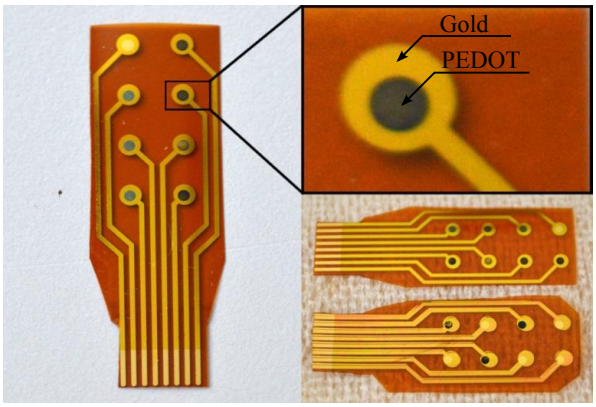

Fig. 1. Gold electrodes with surface area of 1 mm^2 in a flexible substrate, coated with a single layer of PEDOT.

PEDOT is applied by electrodeposition, immersing the electrodes in a solution of the monomer with a specific concentration (C) and a known current (I) for a determined time (t). The charge density (CD) can be adjusted individually and it affects the thickness of the polymeric coating in each contact. We have experimental data for electrodes with charge densities of 40 mC/cm^2, 80 mC/cm^2, 120 mC/cm^2, and also for uncoated gold electrodes which are used as reference.

The surface area (A) is constant for the eight electrodes in each sample. We have experimental data for electrodes with a surface area of 0.5 mm^2, 1.0 mm^2 and 2.0 mm^2.

A. Experimental setup

The polymer-coated electrodes are immersed in an aqueous solution with ionic conductivity, representing the tissues at the implant site. An alternating square voltage of 50 mV is applied at frequencies between 20 Hz and 1 MHz, to obtain the impedance curves as a Bode or a Nyquist plot.

B. *Experimental data and additional measurements*

Experimental results were published by R. Starbird [1] and contain all the impedance information used to perform the mathematical modeling in this work. Starbird obtained the complex impedance of a set of 96 electrodes with different fabrication parameters.

We fabricated eight additional electrodes, keeping two electrodes as reference, and coating six with charge densities of 20 mC/cm^2 and 60 mC/cm^2, three of each. All the eight electrodes were fabricated in a single substrate and were measured by EIS. The Nyquist diagrams of the new electrodes are shown in Fig. 2. Each curve contains 45 data points.

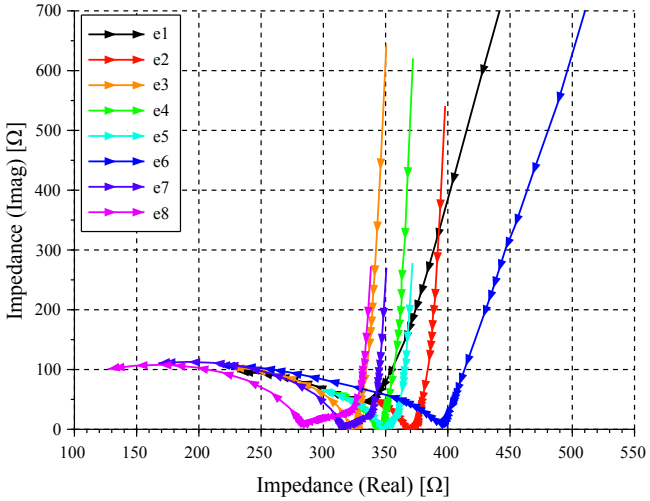

Fig. 2. Nyquist diagram for eight PEDOT-coated gold electrodes.

III. Equivalent Circuit Models for EIS

When the electrode is immersed in an aqueous solution and a voltage is applied, a double-layer of ions establishes in the aqueous media [3]. The electrode potential attracts ions that accumulate close to the polymer, and these ions also attract opposite charged ions to form a second layer.

The double-layer model is a circuit configuration [4] that uses passive components to characterize the interfaces of materials, as can be seen in Fig. 3.

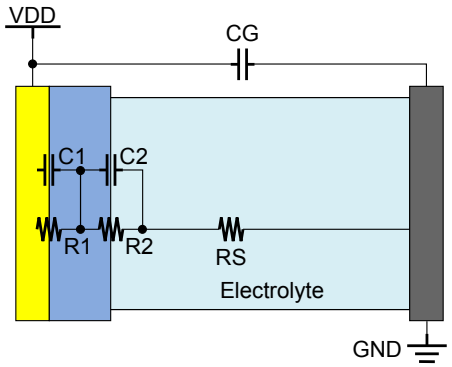

Fig. 3. Physical representation of the double-layer model. The capacitor C2 and resistor R2 describe the double-layer at the solution.

In this configuration, RS is the solution resistance. C1 is the contact capacitance, related with the accumulation of charge between the metal and the polymer. R1 is considered a contact resistance. C2 is the double-layer capacitance, describing the accumulation of charge between the polymer and the solution. Finally, R2 is the reaction resistance, describing the charge transfer between the metal and solution.

The mathematical model presented in Fig. 3 is just one of the possible representations of the physical system. A detailed list of the six mathematical models used in this work to perform the fittings is shown in Fig. 4. This list is a compilation of works from different authors [4–7], with models describing a physical system with a double layer.

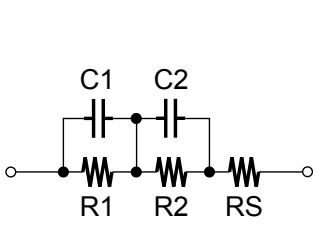

(a) Double-layer model [4].

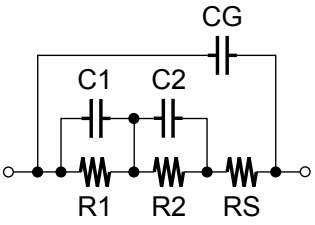

(b) Double-layer with CG [4].

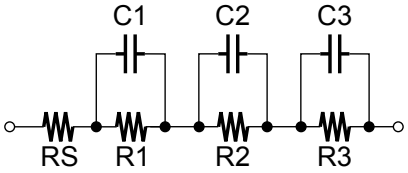

(c) Voigt 3 model [4].

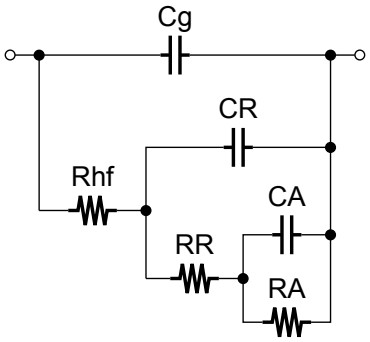

(d) J.R. Macdonald model [5].

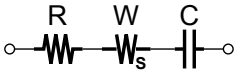

(e) J. Bobacka distributed model [6].

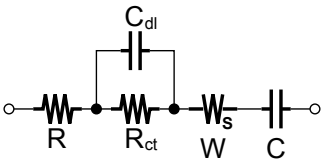

(f) P. Danielsson model [7].

Fig. 4. Mathematical models used in this study.

IV. Experimental Results

Experimental data was fitted to the six equivalent circuit models described in the previous section, using two numerical fitting software programs: LEVMW by J.R. Macdonald [8], and MEISP 3.0 by Kumho Petrochemical Ltd. [9]. Both programs are based on the Levenberg-Marquardt algorithm.

The fitting is performed to obtain information of the detailed parameters of the interfaces. Fitting results are presented in Fig. 5 for a single electrode of 1.0 mm^2 with charge density of 20 mC/cm^2, together with the measured data from EIS. Results for the DL, DLCG and Macdonald model are overlapped.

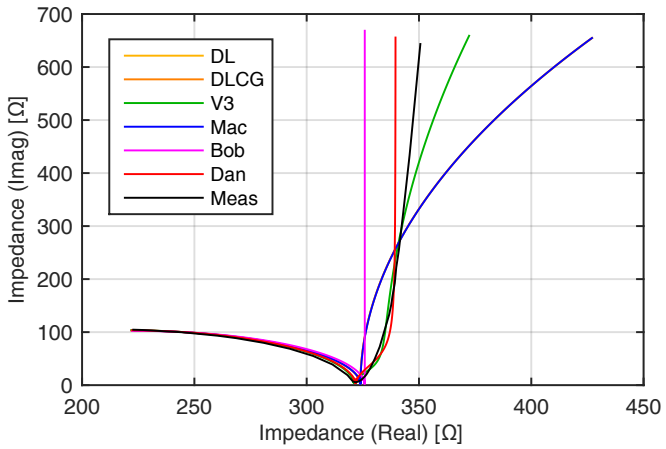

Fig. 5. Fitting results of the six equivalent models, plotted together with the measured data (black curve) for an electrode with surface area of 1.0 mm^2 and charge density of 20 mC/cm^2.

The chi-square goodness-of-fit is computed using the ZView 3.4c software [10] and the results are presented in Table I. The sum of squares (ss) is proportional to the error percentage between measurements and simulations.

TABLE I. Chi-square statistics for the model fittings.

Model	χ^2	ss
Double-layer	0.0016554	0.041384
Double-layer CG	0.0016711	0.040107
Voigt 3	**0.00026523**	**0.0061003**
J.R. Macdonald	0.0016711	0.040107
J. Bobacka	0.0030585	0.079522
P. Danielsson	0.00031711	0.0076107

A. Double-layer capacitance

The double-layer capacitance (C_{dl}) is an element present in the polymer/electrolyte interface. Charge is accumulated at the surface of the polymer, and a double-layer of ions is established in the aqueous media [3].

This parameter increases linearly with the charge density used during the polymerization. This behavior can be appreciated in Fig. 6 for all the studied models. The correlation coefficient R^2 is calculated for 1.0 mm^2 electrodes, after discarding the values closer to zero, because they do not have physical significance. The trend line for linear regression is shown as a red line.

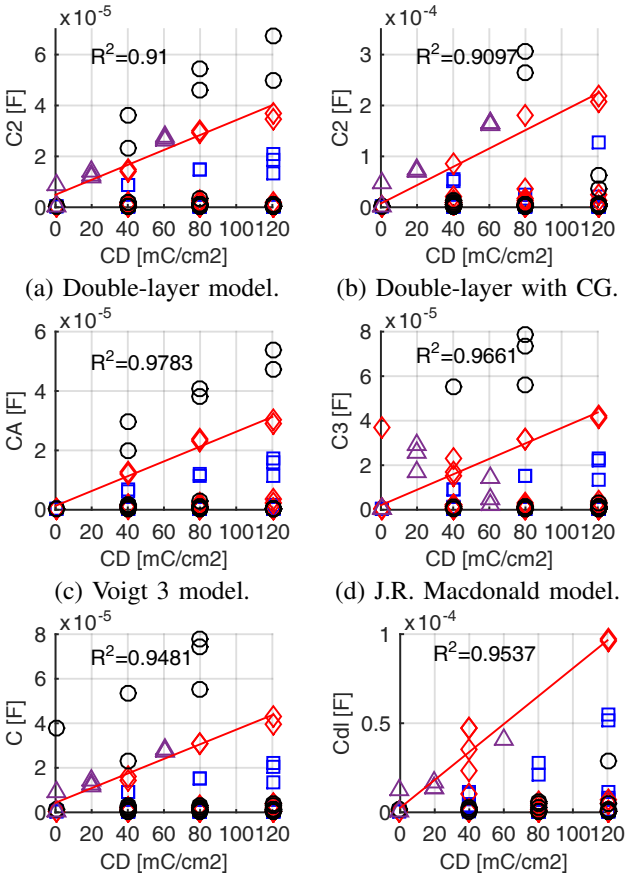

Fig. 6. Double-layer capacitance as a function of the charge density, for electrodes with surface area of 0.5 mm^2 (blue square), 1.0 mm^2 (red diamond), 2.0 mm^2 (black circle), and new electrodes of 1.0 mm^2 (purple triangle) using six different mathematical models.

The fitting results from Fig. 6 suggest that the charge density is affecting the double-layer capacitance. This can be verified by a 1-way ANOVA analysis. We computed the ANOVA statistics for this double-layer capacitance as a function of the charge density in Table II.

The null hypothesis of ANOVA is that the mean values of all the groups are equal, independent from the charge density. Since $p < 0.05$ for all our models, the null hypothesis can be rejected with a confidence level of 95% and we can conclude that the charge density is one parameter actively affecting the value of the double layer capacitance parameter.

TABLE II. ANOVA statistics for the double-layer capacitance as a function of the charge density.

Model	F	p
Double-layer	6.75	2.13×10^{-3}
Double-layer CG	6.39	1.58×10^{-3}
Voigt 3	2.09	1.41×10^{-1}
J.R. Macdonald	9630	3.58×10^{-6}
J. Bobacka	**5220**	$\mathbf{8.38 \times 10^{-11}}$
P. Danielsson	64.4	4.01×10^{-6}

B. Solution resistance

The aqueous solution is an ionic conductor, and this conduction process is described by a single resistance in all of the studied models (R_S, R_{hf}, R). Electrodes with higher surface area have lower resistances, shown in Fig. 7.

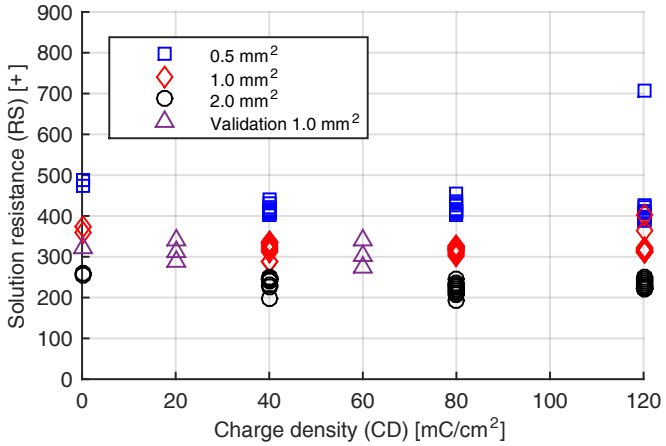

Fig. 7. Solution resistance as a function of the current density, for electrodes with surface area of 0.5 mm^2 (blue square), 1.0 mm^2 (red diamond), 2.0 mm^2 (black circle), and new electrodes of 1.0 mm^2 (purple triangle) using the double-layer model.

V. Discussion

Model fitting was achieved for six equivalent circuit models. The models describe each interface with individual capacitive and resistive parameters. The fitting results are observed in Fig. 5 and the goodness of the fit for each model is presented in Table I. All the mathematical models have almost the same response in high frequencies, and the Nyquist plot from Fig. 5 shows a spread in the low frequency section.

The best fit was achieved with the Voigt 3 model, according to the chi-squared goodness of fit (χ^2=0.00026523), followed by the distributed model of P. Danielsson (χ^2=0.00031711). The chi-squared parameter is proportional to the error between the fittings and the measurements, and the sum of squares reflects the total error percentage difference.

Based on the circuit configurations from Fig. 4, we observe that if the frequency is increased, the capacitors become a short circuit, because the capacitive reactance is reduced. The Warburg element also is short-circuited in high frequencies, and a single resistance R_S or R_{hf} is left alone. This resistance is the solution resistance, plotted in Fig. 7, which proved to be independent of the polymer thickness (ANOVA, p=0.121 $>$ 0.05). From our models we conclude that the impedance of neural electrodes is reduced if the frequency increases, and at high frequencies, the capacitive elements can be neglected and only the solution resistance is observed.

For lower frequencies, capacitances should be taken into account. The double-layer capacitance follows a linear trend as the polymer thickness is increased, with a linear regression correlation coefficient higher than 90% for all the studied models, as seen in Fig. 6. This behavior was expected, because if the polymer is thicker, more charge is accumulated between the polymeric layer and the solution.

The double-layer capacitance shows a linear dependence of the charge density (R2 $>$ 0.9, ANOVA p $<$ 0.05), with the exception of the Voigt 3 model (p=0.141), which provided the best numerical fit but with less physical significance. Electrodes with less surface area presented smaller double-layer capacitances.

VI. Conclusions

In this work, experimental data from 96 electrodes was fitted to six mathematical models. We fabricated eight additional electrodes and compared the goodness of fit using the chi-squared test for all the studied models.

The distributed model from P. Danielsson proved to have statistical significance for both chi-squared and ANOVA tests, and it is the model that describes better our physical system.

At high frequencies, the mathematical models explain the decrease of the impedance, because all the capacitances can be neglected. A single resistance R_S or R_{hf} is left alone in all the studied models. This is the solution resistance, independent of the polymer thickness.

At low frequencies, the double-layer capacitance increases linearly with the charge density.

Acknowledgement

J.J. Montero-Rodriguez thanks the Ministry of Science, Technology and Telecommunications of Costa Rica (MICITT) and the National Council for Scientific and Technological Research (CONICIT) for providing the financial support for this research stay.

References

[1] Starbird, R., Krautschneider, W., Blume, G., and Bauhofer, W. (2013). In Vitro Biocompatibility Study and Electrical Properties of the PEDOT, PEDOT Collagen-Coat, PEDOT Nanotubes and PEDOT Aerogels for Neural Electrodes. In Biomedical Engineering (BioMed 2013), February 13-15, Innsbruck, Austria.

[2] Inzelt, G. (2012). Redox Transformations and Transport Processes. Conducting Polymers, Monographs in Electrochemistry, Springer Berlin Heidelberg, pp. 191-244.

[3] Yang, K., Yiacoumi, S., Tsouris, C. (2004): Electrical Double-Layer Formation. In: Dekker Encyclopedia of Nanoscience and Nanotechnology: CRC Press, vol. 6, pp. 1001–1014.

[4] Yuan, X., Song, C., Wang, H., Zhang, J. (2010). EIS Equivalent Circuits. In Electrochemical Impedance Spectroscopy in PEM Fuel Cells (pp. 139–192). Springer.

[5] Macdonald, J. R. (1992). Impedance/admittance response of a binary electrolyte. Electrochimica Acta, 37(6), 1007–1014.

[6] Bobacka, J., Lewenstam, A., and Ivaska, A. (2000). Electrochemical impedance spectroscopy of oxidized poly(3,4-ethylenedioxythiophene) film electrodes in aqueous solutions. Journal of Electroanalytical Chemistry, 489(1-2), 17–27.

[7] Danielsson, P., Bobacka, J., and Ivaska, A. (2004). Electrochemical synthesis and characterization of poly(3,4-ethylenedioxythiophene) in ionic liquids with bulky organic anions. Journal of Solid State Electrochemistry, 8(10), 809–817.

[8] Macdonald, J. R. (2013). Complex Nonlinear Least Squares Fitting Program. Online at: http://jrossmacdonald.com/. Retrieved on 27.05.2015.

[9] Barsoukov, E. (2014). Impedance Spectroscopy: Evgenij Barsoukov's collection of impedance spectroscopy resources. Online at: http://impedance0.tripod.com/. Retrieved on 27.05.2015.

[10] Scribner Associates Inc. ZView 3.2b. Online at: http://www.scribner.com/. Retrieved on 27.05.2015.